2016

Methcathinone Analogue Activity at the Human Serotonin Transporter

William Drake Varn
Virginia Commonwealth University School of Medicine

Methcathinone Analogue Activity at the Human Serotonin Transporter

A thesis submitted for the partial fulfillment of the requirements for the degree of Master of Science at Virginia Commonwealth University

By:
William Drake Varn
BS Davidson College 2013
Virginia Commonwealth University School of Medicine

Director: Louis J. De Felice
Professor, Department of Physiology and Biophysics

Virginia Commonwealth University
Richmond, Virginia
May 9, 2016

ACKNOWLEDGMENTS

I would like to thank Dr. De Felice for his guidance and direction throughout my road to completion of my masters degree. I would also like to express my sincere gratitude to Dr. Ernesto Solis and Dr. Jose Eltit for directly mentoring me in my research and aiding me with this thesis. In addition, I would like to thank Tyler Steele, and Iwona Ruchala for their consistent support and advice as well as Dr. Steve Negus for serving on my thesis committee.

TABLE OF CONTENTS

List of Figures

List of Abbreviations

NTs	Neurotransmitters
MATs	Monoamine Transporters
5-HT	5-hydroxytryptamine, Serotonin
SERT, hSERT	Serotonin Transporter, Human Serotonin Transporter
DA	Dopamine
DAT, hDAT	Dopamine Transporter, Human Dopamine Transporter
I_{max}	Maximum Current
EC_{50}	Effective Concentration of a Drug that Gives 50% of Maximum Response
LeuT	Leucine Transporter
TM	Transmembrane Protein
S1	Central Binding Site
S2	Secondary Binding Site
Na1, Na2	Sodium Binding Sites
MAOIs	Monoamine Oxidase Inhibitors
TCAs	Tricyclic Antidepressants
SSRIs	Selective Serotonin Reuptake Inhibitors
TEVC	Two-electrode Voltage Clamp
V_M, V_C	Oocyte Membrane Potential, Command Potential
[µM]	Micro-molar Concentration

Abstract

METHCATHINONE ANALOGUE ACTIVITY AT THE HUMAN SEROTONIN TRANSPORTER

William Drake Varn, Master of Science in Physiology and Biophysics

A thesis submitted for the partial fulfillment of the requirements for the degree of Master of Science at Virginia Commonwealth University.

Virginia Commonwealth University School of Medicine, 2016

Director: Louis J. De Felice, Professor, Department of Physiology and Biophysics

In the last few years, there has been continued concern about synthetic drug abuse in both the United States and worldwide. Small adjustments in drug compound structure often allow synthetic drug makers to manufacture a legal product that can produce the same highs as illegal counterparts. Unfortunately, this is happening faster than the government can outlaw the drug compounds, and a wide variety of synthetics are now appearing on the street. This study evaluated the effects on the human serotonin transporter of six different 4-*para* substituted methcathinone compounds. Using a *Xenopus* oocyte model, the efficacy of each MCAT analogue at hSERT was calculated by applying the Hill equation to the oocyte data. This study suggests that volume, size, and steric bulk of the compound may generally influence efficacy at hSERT in a direct manner, but that other factors, like lipophilicity, may also play an important role in potency at the transporter.

Introduction

1.1 Solute Carrier 6 Family (SLC6), Monoamine Transporters

Neurological chemical substances called neurotransmitters are stored in neurons and can be released into the neural synapse. Neurotransmitters cause a myriad of effects in the adjacent neurons and in the presynaptic neuron. These electrochemical events involve neurotransmitters moving through transporters or binding to receptor sites, further propagating a reaction or signal. The human body uses many different chemical compounds as neurotransmitters, including a group named the monoamines. The three monoamines - dopamine, serotonin, and norepinephrine - are derived from aromatic amino acids and contain a two-carbon chain attached to both an aromatic ring and one amino group (Maisto, Galizo, Connors, 2007). The chemical structure of both dopamine and serotonin can be seen in Figure 1, on page 4. The monoamine transporters (MATs) are responsible for the uptake and reuptake of their specific monoamine neurotransmitters to maintain homeostasis within the body (Manepalli *et al*., 2012).

The monoamine transporters belong to the solute carrier 6 (SLC6) gene family. There are 350 solute carrier transporters divided into 55 specific families. SLC6 transporters include the neurotransmitter transporters for GABA and glycine as well as the dopamine, serotonin, and norepinephrine transporters. The polar dipole moments of the amine group make monoamine neurotransmitters lipophobic and therefore they cannot

cross lipid bilayer membranes without the assistance of transporters. The MATs derive the energy to move monoamines against a gradient by coupling the electrochemical potential difference, or cotransport, of extracellular sodium ions and possibly chloride ions. They are therefore sodium dependent transporters and secondary active transporters. More specifically, MATs and all SLC6 transporters are classified as neurotransmitter sodium symporters because the coupled sodium ions move in the same direction, outside to inside the membrane, as the monoamine neurotransmitters (Immadisetty and Madura, 2013). The kinetics of neurotransmitter transporters follow the Michaelis-Menten equation with max turnover rate between 1 and 20 substrate molecules per second and EC_{50} (K_M) values in the low micromolar range (Humphries, Wall, and Rudnick, 1994). The function of chloride in the transport event is still unclear. Many still believe that either one or multiple chloride ions are cotransported with the neurotransmitter substrate and sodium ions (Humphries, Wall, and Rudnick, 1994), but there is no direct evidence to prove this theory. Chloride has been proven necessary for serotonin molecule transport through hSERT, but it may simply be binding at an allosteric site and not actually transported across the membrane with sodium and serotonin (De Felice, 2016). More future experiments are needed to truly understand chloride's distinct role at the monoamine transporters.

Neurotransmitter transporters, including MATs, maintain neurotransmitter homeostasis in neurons by uptake of neurotransmitter into postsynaptic neurons or through reuptake back into the presynaptic neuron. The amount, or density, of transporters in the membrane can be regulated by the cell through up and down-regulation. Adding or removing transporters may modulate the rate at which neurotransmitters are removed from the synapse allowing the cell to control neuronal

activity directly. For this reason, the MATs have been and continue to be drug targets for treatment of many diseases and addictions (Hediger *et al.*, 2003).

All monoamine neurotransmitter transporters share the same unique basic structure. Molecular cloning suggests that on average approximately 40% of the amino acid structure belongs to all neurotransmitter transporters. The human dopamine and serotonin transporters have one single isoform consisting of 617 and 630 amino acids, respectively, in 12 transmembrane helices. Both transporters contain intracellular N- and C-termini, a glycosylated loop between transmembrane helices III and IV, and a pair of Cys residues within extracellular loop 2 forming a N-linked glycosylation site and an intraloop disulfide bridge (Guastella *et al.*, 1990). Due to instability, quantity, and purity difficulties, protein crystallization of SLC6 transporters has been difficult (Immadisetty and Madura, 2013) and some prokaryotic transporter proteins are more stable. The most important of these prokaryote transporters is the leucine transporter (LeuT) because it has shown vast functional resemblance and sequence homology to SLC6 transporters. (Yamashita *et al*. 2005). Recently, X-ray crystallography of the human serotonin transporter bound to two seperate antidepressants was published (Coleman, Green, and Gouaux, 2016). Their experiments identified the central binding site between helices 1, 3, 6, 8, and 10. An allosteric site was shown to modulate ligand binding at the central site (Coleman, Green, and Gouaux, 2016). Due to the novelty of these findings and the vast amount of research performed previously on the leucine transporter, further discussion of transporter structure and function will focus on LeuT.

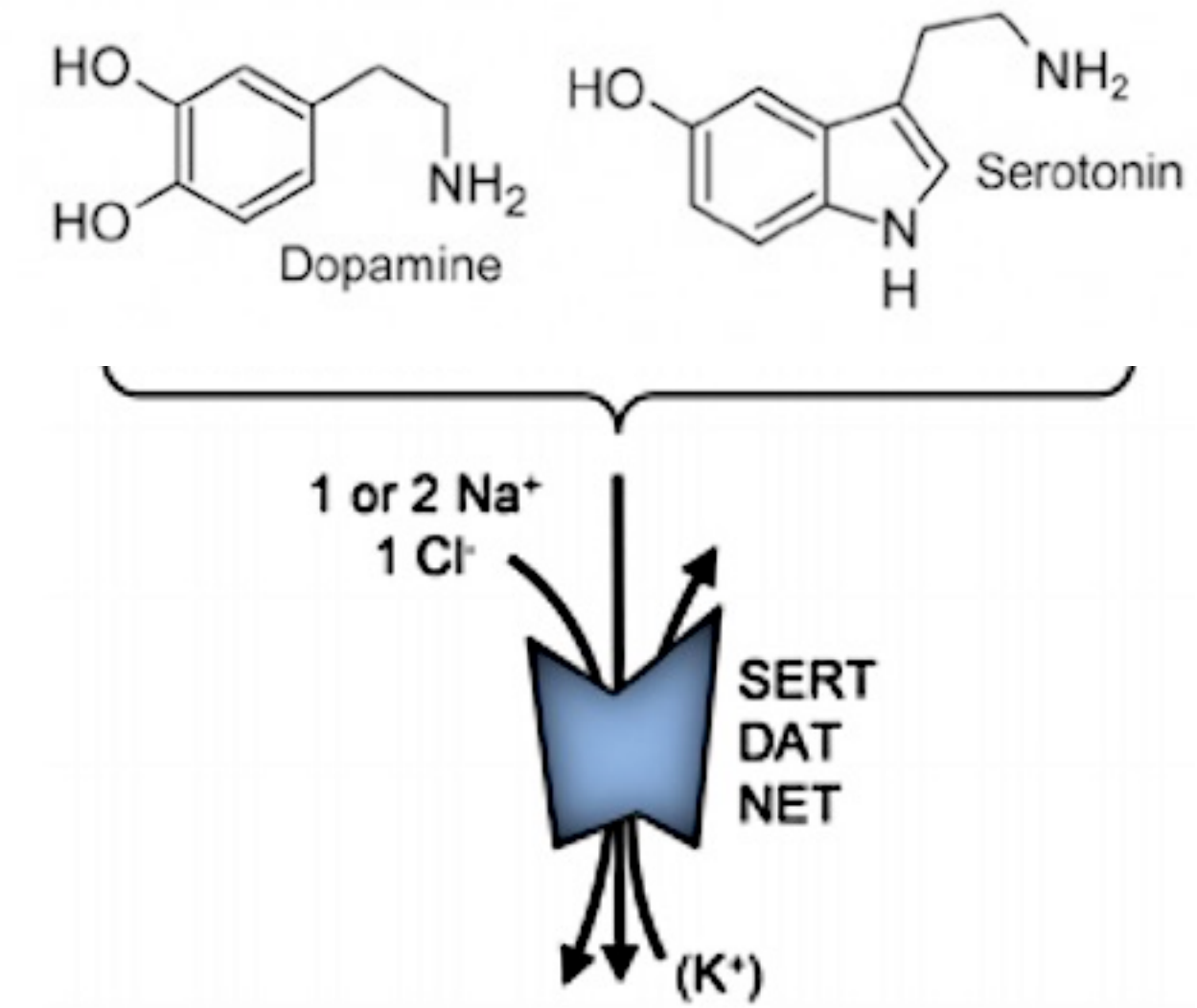

Figure 1.1 : The chemical structure of the SLC6 family monoamines dopamine and serotonin along with an illustrated representation of a monoamine transporter. The illustration also depicts the number of ions thought to travel across the membrane with the monoamines. It is important to note that the role of the chloride ion is still unclear, and Cl^- may not actually be transported across the membrane (De Felice, 2016). (Above figure borrowed from *SCL6 Neurotransmitter Transporters: Structure, Function, and* Regulation by Kristensen *et al*., 2011.)

1.2 The Leucine Transporter, Structure and Relevance to SLC6 Family

The thermophile bacteria *Aquifex* aeolicus possess the leucine transporter, and LeuT shares 20-25% sequence identity with the MATs (Immadisetty and Madura, 2013). Its resemblance has been extensively verified and structures of LeuT have been elucidated, with and without substrates and with competitive and noncompetitive inhibitors. X-ray crystallography of LeuT confirmed the 12 transmembrane helices with internal N- and C-terminus structure and confirmed individual properties of each transmembrane protein's intracellular and extracellular half. For example, the large second extracellular loop and its multiple glycosylation sites seem to play a role in synthesis, trafficking, and stability (Hahn and Blakely, 2007). LeuT also established the cylindrical shape of the helical protein bundle with transmembrane protein 1 (TM1), TM3, TM6, and TM8 making up the inner ring, forming a distinct central binding pocket (S1) for substrates. TM1, TM3, TM6, and TM10 contain side chains that interact in a network to block the S1 binding pocket from external media. The intracellular halves of TM1, TM6, and TM8 form the second half of the gating region; a large tight protein network covering the S1 binding site on the intracellular side. In order for a substrate to bind, these protein regions must undergo structural rearrangement in a sequence of conformational states. These regions are consistent throughout the SLC6 family, except for one glutamate replacing Asp404 in the serotonin transporter (Yamashita *et al.,* 2005; Kristensen *et al*. 2011).

The overall asymmetric LeuT structure, called the "5+5 inverted repeat", is not consistent with the structure of SLC6 transporters, but it is believed that LeuT's central binding site (S1) and sodium ion binding sites are equivalent to the corresponding sites

within SLC6 transporters; the four-helix bundle comprising these sites shares 55-67% sequence similarity. This discovery established the LeuT homology model for neutrotransmitter transporters and has allowed reputable 3D models of human DAT and SERT. The model does retain limitations; while the inner and outer ring regions are overall analogous, the intra- and extra-cellular loop regions and the short N- and C- termini of LeuT differ from the SLC6 counterparts (Yamashita *et al.,* 2005; Kristensen *et al*. 2011).

The S1 pocket consists of two distinct regions. First, TM1 and TM6 form a polar region that can contain the charged α-amino and α-carboxylate groups of the amino acid substrate. These alpha groups form hydrogen bonds with available amide groups on TM1 and TM6. The second section of the S1 pocket consists of hydrophobic sections of TM1, TM3, TM6, and TM8 in order to accommodate a substrate's aliphatic hydrophobic side chains. This second portion plays a large role in binding specificity of substrates in S1.

Molecular dynamics have suggested the presence of another binding site in LeuT, the S2 binding site, within the solvent-accessible path from extracellular media to the S1 site and separated by an extracellular gate. Various LeuT inhibitors have been found bound in the S2 site, preventing necessary conformational changes allowing substrate movement to the intracellular side. It has thus been proposed that occupation, or possibly a lack there of, in the S2 site is required to initiate conformational movement required for substrate to enter the cell. The S2 site control of S1 alludes to a possible SLC6 transporter inhibitor mechanism of action (Singh *et al*. 2007; Yamashita *et al*. 2005). The recently published hSERT crystal structure studies by Coleman, Green, and Gouaux confirms the notion of an allosteric site in hSERT. Using electron density mapping, the studies showed citalopram bound in an allosteric site that is distinct in hSERT and not present in hDAT.

Mutations to this allosteric site resulted in markedly decreased potency of citalopram binding, but the resulting effects on substrate transport are still unclear (Coleman, Green, and Goax, 2016). A structural representation of S1 and S2 can be seen in Figure 2, on page 9.

In addition to the S1 and S2 binding sites, there are also two sodium ion-binding sites in LeuT. The two sites, Na1 and Na2, are both located within the S1 binding pocket. The sodium bound in the N1 site interacts with the α-carboxyl group of the transporter substrate and this is believed to be the first step towards translocation of both into the cell. Both Na1 and Na2 serve to stabilize TM1 and TM6 in the presence of substrate by organization with side-chain oxygens and backbone carbonyls, five for Na1 and eight for Na2 as can be seen in Figure 3. The structure of SERT illustrates the conservation of residues surrounding the sodium ion binding sites throughout the SLC6 transporter family, because an Asp in monoamine transporters exchanged for Gly24 in LeuT is the only structural difference between LeuT, DAT and SERT. It is less clear whether or not the Na2 site is structurally and functionally identical to LeuT and the SLC6 transporters. Five different residues make up Na2 in LeuT, of which one is identical and three are very similar in the SLC6 family. Multiple theories have been proposed about the roles of both the Na1 and Na2, but some human neurotransmitters only translocate one sodium ion and others two. Only speculations can be made to the exact function of Na1 and Na2 due to discrepancies across the SLC6 family regarding these sites, and a current lack of functional data (Singh *et al.* 2007; Kristensen *et al*. 2011).

Figure 1.2 (right) : A computer generated illustration of the S1 and S2 binding pockets in LeuT. The different transmembrane domains that construct the binding pockets can also be seen. The yellow spheres represent a leucine within the main substrate binding pocket.

(Above figure borrowed from Kristensen *et al*., 2011.)

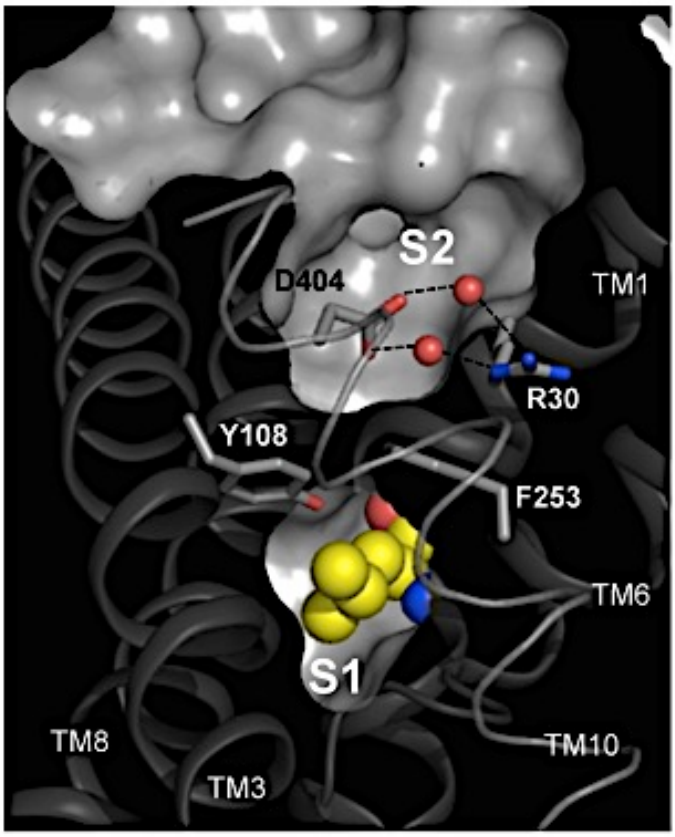

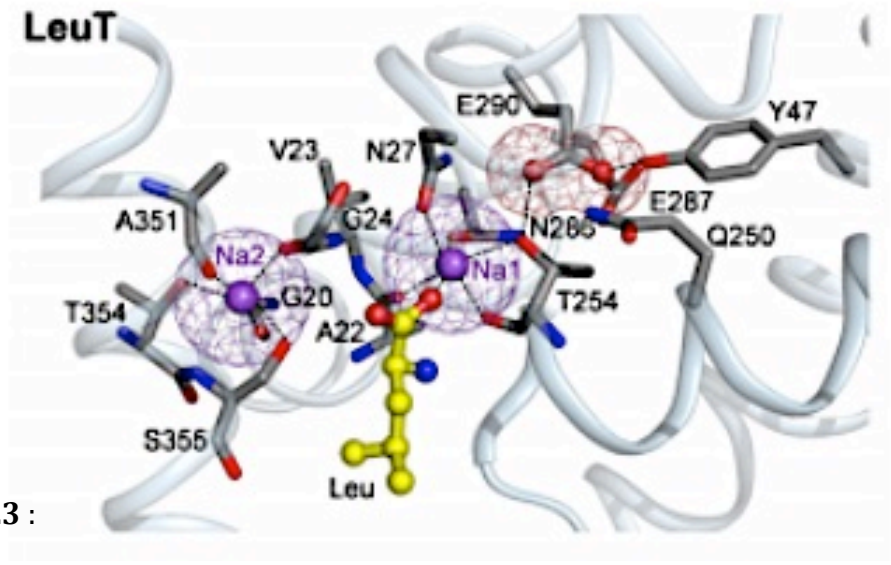

Figure 1.3 :

The leucine transporter's Na1 and Na2, shown in purple, stabilize TM1 and TM6 by organization with side-chain oxygens and backbone carbonyls; five for Na1 and eight for Na2. (Figure 3 also borrowed from Kristensen *et al*. 2011).

1.3 MAT Mechanism of Action - Alternating Access Model

The first model of transport mechanism was proposed in the late 1950s, then was adjusted and named the "alternating access" model about a decade later. Supporters of the alternating access theory believe that secondary active transporters have three main conformational states. First, the substrate binding site is exposed to the external media. Next, the binding site is internalized and blocked from all media. Finally, the binding site is exposed to the internal media. This model suggests impermeable gates, or a gating like action, on the external and internal sides that can be closed as the transporter transitions through conformational states to move substrate into or out of the cell (Jardetzky, 1966; Mitchell, 1990). Early research indicated multiple TM regions and residues undergo conformational change and move positions, possibly substantiating the alternate access model and making it the widely accepted basis for transport mechanism. The discovery of LeuT's stable nature for testing, structure, and relationship to the SCL6 family and monoamine transporters has begun offering glimpses of various transporter conformations. LeuT has been shown in the outward-facing conformation but not the inward-facing conformation, though other prokaryotic transporters sharing LeuT's '5+5 inverted repeat' folding have been crystalized in both. For example, a sodium-benzylhydantoin symporter (Mhp1), a carnitine-butyrobetaine aintiporter (CaiT), an arginine-agmatine symporter (AdiC), an H^+-coupled amino acid symporter (ApcT), and a sodium-galactose symporter (vSGLT) all share the 5+5 repeat and have been crystalized in multiple conformations. All five hail from five different transporter families, though this apparent conservation of structure across transporters has corroborated the theory that

the related SCL6 family of transporters operates by the same mechanisms (Forest and Rudnick, 2009; Kristensen *et al*. 2011).

Multiple models of the alternating access transport theory have been proposed, and each begins with the initial step of substrate binding in the S1 site. Experiments with LeuT and competitive inhibitors indicate that once the substrate has entered through an extracellular permeation pathway and bound to its proper site, a transition begins (Malinauskaite *et al.*, 2014; Stolzenberg *et al*., 2015). The substrate becomes completely occluded in an intermediate step, thanks to external portions of TM1, TM3, TM6, TM8, TM2, and TM10 rearranging to form the extracellular gate. Next, a pathway forms between the inner ring portions of TM1, TM6, and TM8 so that the substrate can be released and diffuse into the cell. The second step, transitioning to the intracellular pathway, requires much more movement and translocation than the first step of just closing the extracellular gate. How exactly this happens is unclear, but one theory states that TM1 and TM6 hinge in the middle, allowing their unwound end segments to block extracellular and intracellular media when appropriate (Malinauskaite *et al.*, 2014; Stolzenberg *et al*., 2015; Billesbølle *et al*., 2015). A contrasting model proposes a more inflexible rocking motion between the outward and inward conformations due to TM1 and TM6 interacting with TM2 and TM7 in an inelastic fashion. And still, another speculation involves TM1 and TM6 rearranging counterclockwise with TM8. While there has been a recent surge in research on SCL6 transporters and monoamine transporters, a deficiency in protein dynamic experimental data still presents issues correlating proposed structural mechanisms with actual transporter function (Beuming *et al.*, 2006).

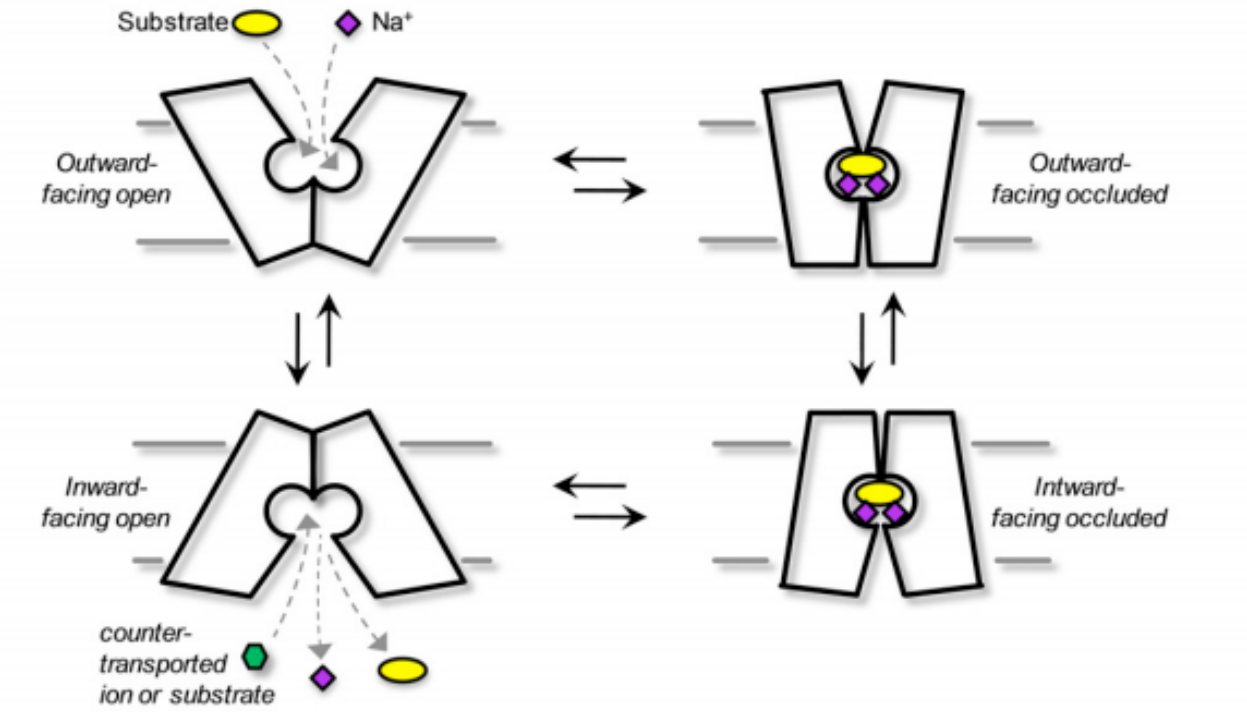

Figure 1.4 : A visual representation of the four possible conformations involved in the alternating access model of substrate transport. Each conformation can change in one of two ways, either releasing the substrate, or holding it within the binding pocket – one theory of how the transporters employ a gating mechanism (Figure 4 borrowed with much thanks from *SCL6 Neurotransmitter Transporters: Structure, Function, and* Regulation by Kristensen *et al*., 2011). It is important to note that this model of transport would not result in the currents seen in TEVC, and therefore there must be another mechanism of transport acting instead, or along side, the alternating access model.

1.4 MAT Mechanism of Action – Transporter Channels

As data and analysis of transporter action have improved, the partition between active transporters and passive ion channels has begun to get cloudier. After the discovery of co-transporters, many believed that electrodiffusion was not a sufficient mechanism for concentrating against a gradient. These researchers and scientists thus presented transporters in a more enzymatic scheme, based on radiolabeled uptake experiments, giving rise to the alternating access model. The disagreeing group stuck to electrical measures and experiments, creating a contrasting theory of electrodiffusion governed channels as a mechanism for transporters. More recently developed experimental methods, such as single channel patch clamp and the cloning of co-transporters, have revealed that the true mechanism of transporters might be a combination of both ideas (De Felice, 2004).

Dr. L. De Felice has proposed that co-transporters might actively follow the enzyme theory, but under the correct conditions the transporter may open into a passive channel mode. Co-transporters could act as channels while using flux coupling to drive secondary activity. Flux coupling takes place when a channel is too narrow to allow the substrate and ion to pass each other. If the ion flow down its gradient is dominant enough, it can force the substrate against its own gradient (De Felice, 2004). Thanks to convincing experiments beginning in the 1990s, the presence of a channel in transporters is well documented, though the purpose and function of the channel is still unclear.

In a 2007 review paper, De Felice and Goswami made a compelling argument for the presence of a channel in monoamine transporters. Dopamine and serotonin transporters

generate a current because the membrane crossing substrates and sodium carry a positive charge, which is only partially offset by chloride's negative charge. The movement of all three across the membrane creates a current that can be quantified by the equation:

$I = Nvq$

in which "I" is the current, "N" is the number of transporters, "ν" is the cycle rate, and "q" is the net charge transferred with each cycle of the transporter. A single 5HT substrate molecule has a +1 charge for the equation above (1 $5HT^+$, 1 Na^+, 1 Cl^-). If one million transporters operate in an alternating access like fashion at one cycle per second with a transfer of +1 charge for each cycle, 0.16 pico-amps of current would be generated per second (De Felice and Goswami, 2007). Flash photolysis and whole cell patch clamp techniques have shown that the total current across the membrane due to serotonin transporters alone falls in the hundreds of pico-amps (Bruns *et al*., 1993). This large discrepancy clearly points to another mechanism taking place and a transporter channel function could create the much greater current.

1.5 Monoamine Transporters & Drugs

Despite our lack of molecular understanding of MATs' functional mechanisms, drugs have been used for years to manipulate these channels and neural activity. Currently there are more than 30 drug compounds available that affect MATs. Many more have been developed but not made it to market due to lack of efficacy or side effect consequences.

Two sets of drugs, the monoamine oxidase inhibitors (MAOIs) and tricyclic antidepressants (TCAs), were discovered and used to treat patients as far back as the 1950s. These drugs are not specific and modulate multiple neurotransmitters. Neither are first line medications today due to a myriad of side effects. Like the name suggests, the MAOIs inhibit the monoamine oxidase enzyme, which breaks down monoamines in the synaptic cleft. MAOIs affect dopamine, serotonin, and norepinephrine. A limited tyramine diet is required, or MAOIs can cause hypertensive crisis. The tricyclic antidepressants were discovered a few years after the MAOIs and were then implemented as first line treatment for many years. TCAs primarily block reuptake of 5-HT and norepinephrine, but also block muscarinic M1 receptors, histamine H1, and alpha-adrenergic receptors. This lack of specificity causes dose related side effects like cardiac effects, anticholinergic and antihistamine effects, decreased seizure threshold, sexual disfunction, diaphoresis, and tremor (Hirsch and Birnbaum, 2015 [1]). Despite the wide range of possible adverse effects, many people still safely use tricyclics today.

Currently, selective serotonin reuptake inhibitors (SSRIs) are more typically given to treat depression or other psychiatric disorders. The FDA approved fluoxetine in 1987 as the first SSRI safe for treatment and there are now 6 different commonly prescribed SSRIs.

Besides depression, SSRIs can alleviate panic disorders, obsessive-compulsive disorders, PTSD, general and social anxiety, many eating disorders, and premenstrual dysphoric disorder. It is believed that SSRIs inhibit the cytochrome P450 hepatic enzyme which metabolizes many substances, and therefore adverse drug interactions are possible when taking SSRIs. SSRIs reach peak plasma levels within eight hours of being absorbed by the GI tract and are thought to reduce 5-HT reuptake activity by 60 to 80 percent. Unfortunately, the full therapeutic effects of SSRIs are not typically realized for 3 to 8 weeks after initial consumption. Many attribute this to SSRIs' downstream effects and slow increase in neuroprotective proteins (Hirsch and Birbaum, 2015 [2]).

More recent drug discovery has produced a selective dopamine reuptake inhibitor called bupropion, dual-acting inhibitors like selective serotonin and norepinephrine reuptake inhibitors (SNRIs, ex: duloxetine), dopamine and norepinephrine inhibitors (ex: nomifensine), and compounds that inhibit all three monoamine transporters (ex: tesofensine). Cocaine is also a nonselective reuptake inhibitor at all three transporters. Cocaine is most commonly associated with dopamine because it is more efficacious at hDAT than hSERT, and because it is believed that DAT causes addiction properties (Carroll, 2003; Jin *et al.*, 2008). Most illegal drugs elicit some degree of modulation at each monoamine transporter. The relevant drugs are discussed below in the individual DAT and SERT chapters.

1.6 Human Serotonin Transporters (hSERT)

Serotonin, or 5-hydroxytryptamine (5-HT), transporters are best known for their effects in the central nervous system, but these transporters are also located in the enteric nervous system, in specialized neuronal cells, and in placental syncitiotrophoblasts (Blakely *et al*., 1998). Outside of the CNS, serotonin plays a role in regulating cardiovascular function, bowel motility, energy balance and food intake, endocrine function, and some genitourinary effects. At least 15 different serotonin transporters have been identified and grouped into seven families based on signaling mechanisms. This plethora of receptors in various locations explains why sometimes side affects like diabetes, metabolic syndromes, and valvular heart disease can occur with serotonergic drugs (Berger *et al*., 2009).

All brain regions express multiple serotonin receptors, and even individual neurons can express multiple 5-HT receptors. Serotonin, an indolamine neurotransmitter released from neurons originating in the raphe nuclei, modifies anger, aggression, appetite, attention, mood, perception, reward, and sexuality. Each serotonin receptor subtype can affect one or many different brain processes (Berger *et al*., 2009). 5-HT plays a role in many related mental illnesses including depression, obsessive-compulsive disorders, anxiety, eating disorders, autism, schizophrenia, and alcohol abuse. Many attempts have been made to link SERT, or a lack of 5-HT and SERT, to impulsivity and the diseases listed above. At this time no conclusive data has been shown (Hahn and Blakely, 2007).

The human serotonin transporter is encoded by the SCL6A4 gene. SERT knockout mice have been engineered by altering this gene. The knockout mice display an increase in

extracellular 5-HT and a decrease in 5-HT tissue content, despite the overall level of 5-HT biosynthesis remaining constant (Bengel *et al*., 1998). These results suggest that the transporter is, in fact, the main mechanism by which the body removes released 5-HT and by which cells reclaim 5-HT for intracellular stores. These results have also been seen when 5-HT reuptake inhibitors are administered during early development, linking development, 5-HT homeostasis, and adult anxiety-related behavior (Bengel *et al*., 1998).

Variations in the promoter region, located 1 kilobase upstream, modify human SERT expression. There are two polymorphisms defined by the presence or absence of a 44-base pair group in the promoter region: the short allele and the long allele. Two single-nucleotide polymorphisms have been shown to slightly modify transcriptional activity, but transcriptional activity is mainly determined by short versus long allele, with the short having a lower transcriptional activity. Some data suggest that humans who possess the short allele are more predisposed to depression in response to stress, and are more likely to demonstrate neuropsychiatric conditions [ex: autism, OCD, eating disorders] and anxiety-related personality traits (Kristensen *et al*, 2011; Hahn and Blakely, 2007). Other preliminary data suggest that the short allele limits the affects of selective serotonin reuptake inhibitors (SSRIs) in depressed patients due to the lack of SERT. The longer allele causes proper transcription of SERT, but may predispose to hypertension through an unknown mechanism of SERT located on blood platelet cells (Hahn and Blakely, 2007; Eddahibi *et al*., 2001).

In addition to the long and short allele, other variants have been found. The I425V variant is associated with obsessive-compulsive personality disorder and, interestingly, increases uptake compared to wild-type. It has been proposed that either altered surface

expression or enhanced intrinsic transport capacity causes this difference in uptake ability (Kilic *et al*., 2003; Prasad *et al*., 2005). Five different short-nucleotide polymorphisms (SNPs) have been acknowledged in relation to autism. These SNPs cause mutations in the coding region of the SERT gene and, similar to the I425V variant, result in an increase in SERT expression and uptake levels. A third variant, the K201N variant, has increased glycoslylation and has been shown to increase SERT expression levels by thirty percent (Kristensen *et al*., 2011; Rasmussen *et al*., 2009).

Mechanism	Drugs Involved
Increases Serotonin Formation	Tryptophan
Monoamine Transporter Substrates	Amphetamines (including dextroamphetamine, methamphetamine) MDMA (Ecstasy) Amphetamine derivatives (including fenfluramine, dexfenfluramine, phentermine) Levodopa, Carbidopa-levodopa (indirectly)
Monoamine Transporter Inhibitors	Cocaine Selective Serotonin Reuptake Inhibitors (SSRIs) (including citalopram, escitalopram, fluoxetine, fluvoxamine, paroxetine, sertraline) Serotonin-Norepinephrine Reuptake Inhibitors (SNRIs) (including desvenlafaxine, duloxetine, milnacipran, venlafaxine) Dopamine-norepinephrine reuptake inhibitors (including bupropion) Serotonin modulators (including nefazodone, trazodone, vilazodone) Tricyclic Antidepressants (TCAs) (including amitriptyline, amoxapine, clomipramine, desipramine, doxepin, imipramine, maprotiline, nortriptyline, protriptyline, trimipramine) St. John's Wort (*Hypericum perforatum*)

Monoamine Transporter Inhibitors (Continued)	5-HT3 receptor antagonists (dolasetron, granisetron, ondansetron, palonosetron) Valproate Sibutramine
Inhibits Serotonin Metabolism (inhibits monoamine oxidase activity)	Monoamine oxidase inhibitors (MAOIs) (including phenelzine, tranylcypromine, isocarboxazid, moclobemide, selegiline, rasagiline, linezolid, tedizolid, methylene blue, procarbazine, Syrian rue)
Direct Serotonin Agonist	Lorcaserin Buspirone Triptans (including sumatriptan, rizatriptan, others) Ergot derivatives (including ergotamine, methylergonovine) Fentanyl Lysergic acid diethylamide (LSD)
Increases Sensitivity of Postsynaptic Serotonin Receptor	Lithium

Table 1.5 : List of mechanisms affecting serotonin and SERT, and also the drugs that elicit each mechanism.
(adapted from UpToDate.com "Examples of drugs that can precipitate serotonin syndrome" http://www.uptodate.com/contents/image?imageKey=EM/64604&topicKey=PSYCH%2F14675&source=outline_link&search=ssri&selectedTitle=1~150&utdPopup=true)

1.7 Xenopus Oocytes and RNA Expression

The *Xenopus laevis*, or African clawed frog, originally populated areas south of the Sahara desert along the African Rift Valley, but today are found all over the world in stagnant pools and streams. This species of frog can live up to fifteen years and is sexually mature ten to twelve months after birth. Each female can mate up to four times a year, and mating is most common in spring and summer. They lay between five hundred and two thousand spherical eggs at once, each 0.04 inch (0.1 cm) in diameter. Each female can produce and lay up to 8,000 eggs a year, making the frogs and their eggs a viable, inexpensive, and efficient research model for many experiments (nationalzoo.si.edu).

The Xenopus oocyte's large size makes them easy to handle in electrophysiology models under a microscope. The oocyte possesses a resting membrane potential between -50 and -60 mV, due mainly to the permeability of K^+ ions (nationalzoo.si.edu). After fertilization occurs, the oocytes prepare for the upcoming developmental stages by producing and storing organelles, enzymes, and proteins. Electrophysiology takes advantage by influencing the oocyte to produce choice proteins of interest.

Human RNA cannot simply be injected into the oocyte and be expressed. The RNA template must first be placed into a Xenopus oocyte compatible vector, so the cDNA of SERT and DAT was subcloned into a pOTV vector, or Oocyte Transcription Vector. Afterward, mRNA can be prepared *in vitro* from the cDNA and this RNA can be injected into the oocyte. The human protein located within the pOTV will now be synthesized, assembled, and targeted to the oocyte membrane (Miller and Zhou, 2000). Typically,

between 10^7 – 10^{10} new proteins will be expressed in each cell's membrane (Sigel, 2010). A summary of the oocyte process can be seen in the figure below.

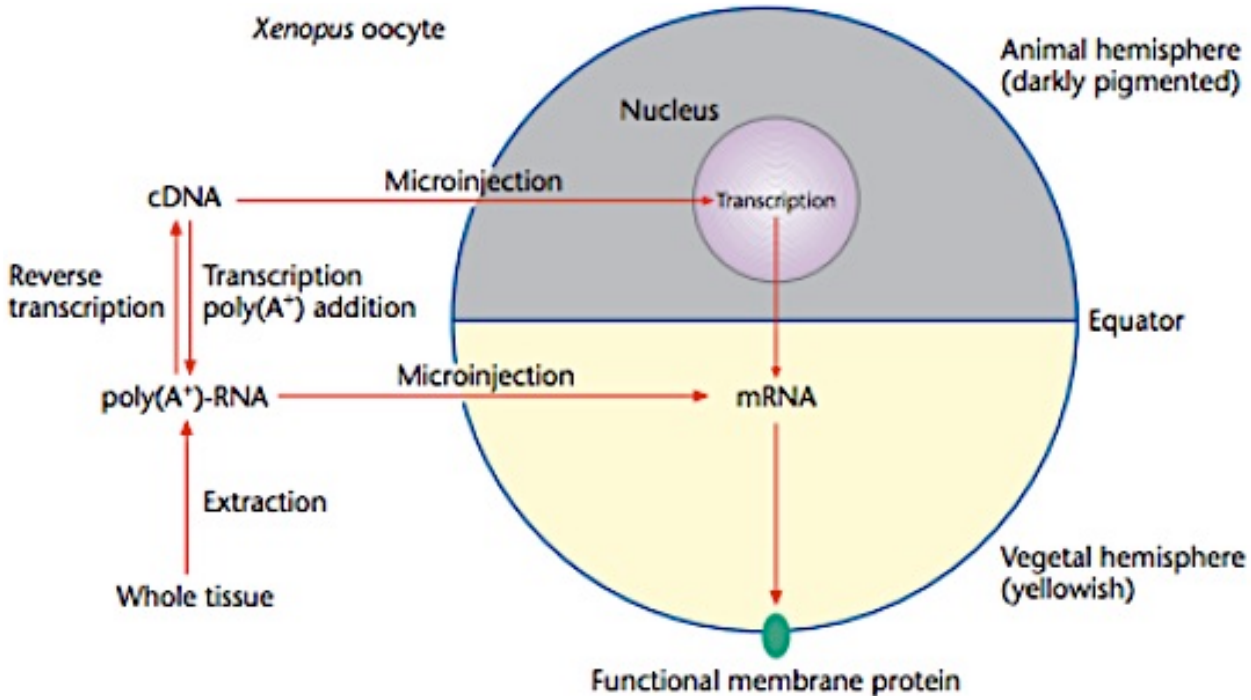

Figure 1.6 : A summary of the steps necessary to express membrane proteins in *Xenopus* oocytes, beginning with nucleic acid extraction from tissue. It is worth noting that in our synthetic cathinone experiments human MAT RNA was injected into the vegetal hemisphere only, though microinjection into the animal hemisphere is also possible, as shown (Figure borrowed from E. Sigel's 'Microinjection into Xenopus Oocytes', 2010).

1.8 Two-Electrode Voltage Clamp

The most common electrophysiological technique used with exogenous mRNA expression in *Xenopus* oocytes is two-electrode voltage clamp, or TEVC. TEVC has provided the majority of our ion channel property data and understanding. Two-electrode voltage clamp permits the study of ion channels, or other electrogenic membrane proteins, by controlling the oocyte membrane potential (V_M). This technique can be used with voltage-dependant ion channels, or with ligand-gated ion channels. In our case, the DAT and SERT transporters are ligand gated transporters and TEVC tracks the electrical potential changes across the membrane due to ion and substrate [neurotransmitter or drug] movement (Guan *et al.*, 2013).

The asymmetrical ion distribution across the cell membrane causes an electrochemical gradient, and this difference gives rise to the membrane potential. This gradient and potential are due to a host of ions, each of which demonstrate varying permeability dependent upon the particular environmental conditions. The Goldman-Hodgkin-Katz equation is pertinent to this research because it describes how ion permeability and changes in the permeability change the overall membrane potential. In order to use the equation one must assume that there is free diffusion across the membrane, that the diffusion coefficient (D_C) remains constant, and that the electrical field within the membrane remains constant (Bierwirtz and Schwarz, 2014). If these conditions are met, the Goldman-Hodgkin-Katz equation for Na^+, K^+, and Cl^- can be given by:

$$E_{GHK} = (RT/F) \ln [(P_{NA}[Na]_{out} + P_K[K]_{out} + P_{Cl}[Cl]_{in}) / (P_{Na}[Na]_{in} + P_K[K]_{in} + P_{Cl}[Cl]_{out})]$$

where *R* is the universal gas constant, *T* is the absolute temperature, and *F* is the Faraday constant.

The opening and closing of ion channels govern the resistance characteristics of the cell membrane, and therefore current-voltage (IV) properties describe functions of the transporters in the membrane (Bierwirtz and Schwarz, 2014). Two-electrode voltage clamp employs two electrodes, both inserted into a large cell with low resistance (oocyte). The first electrode injects a varying current, the command potential (V_C), into the cell maintaining a desired value; in this case it maintains the cell's resting membrane potential (V_M) of approximately -60mV. The second electrode, the potential electrode, measures how much current must be injected into the cell to keep the desired value (Guan *et al*., 2013). Figure 6 below further displays the basic theory and workings of TEVC.

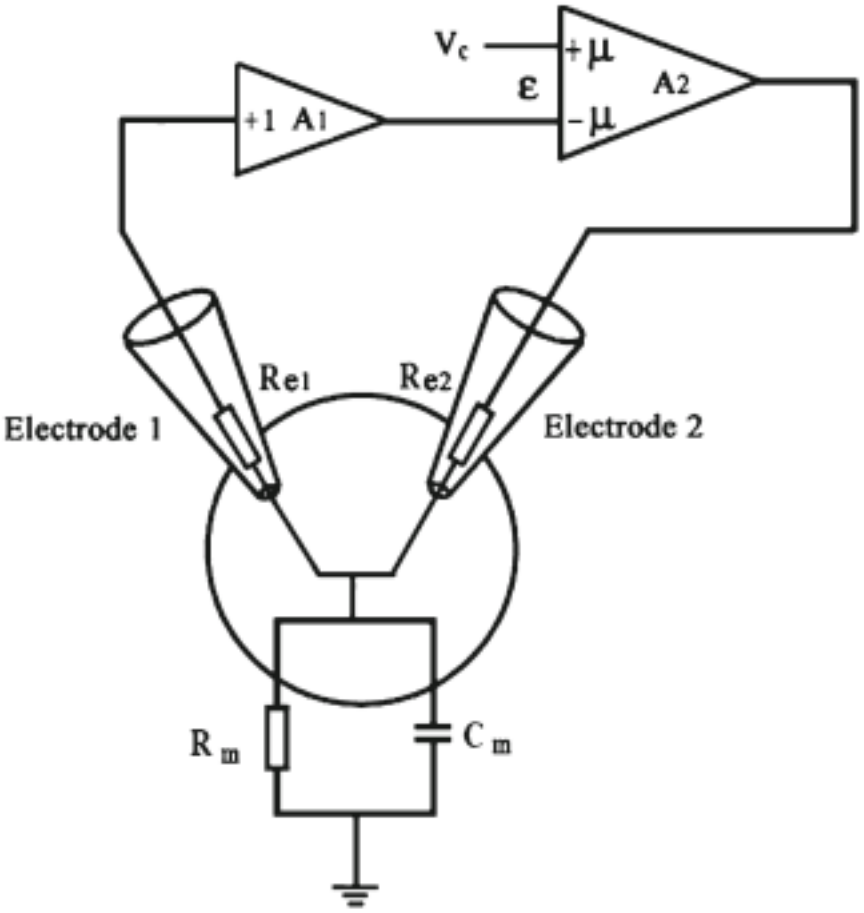

Figure 1.7 : Conventional two-electrode voltage clamp (TEVC) on an oocyte (borrowed from Guan *et al*., 2013). A1 is a voltage follower with high input impedance and low resistance that monitors V_M. A1's output equals V_M and is measured by the connected clamping amplifier, A2. A2 compares the measured V_M to V_C, the voltage command signal, which is applied to the other input terminal. ε is the current output of A2, which is a current proportional to the difference between V_M and V_C. This current flows through the current electrode, electrode 2, and into the cell. V_M clamping is achieved when V_M nears V_C. The current passing through electrode 2 counterbalances V_M deviations and is therefore measured as the membrane current (Guan *et al*., 2013).

1.9 Cathinone, Methcathinon, and Analogues

An underground market of synthetic psychoactive substances has emerged and thriven within the last decade. The Unites States' and European Union countries' laws prohibiting conventional illicit drugs drive many individuals to seek other legal substances that produce the same effects. These new synthetic compounds are often synthesized by clandestine chemists, but some can even be cooked by individuals with little chemistry background. When made correctly, synthetics elicit the desired affects but they also are often very toxic in higher doses. For example, synthetic cannabinoids or "spice", activate endocannabinoid receptors similar to cannabis, and synthetic cathinones or "bath salts", activate pathways similar to cocaine and amphetamines. When taken in excess, drugs such as these can cause violent behaviors and many health problems including hallucinations, agitation, psychosis and death (Baumann *et al*., 2014). Recently, a man in Florida attempted to cash a check for 386 billion dollars, and another individual turned himself in to police for "murdering his imaginary friend." While these two stories could easily be fabricated, the media suggested that both men ingested toxic amounts of bath salts prior to these events. True or not, these are two of the many events associated with bath salt intoxication pushing governments to outlaw known forms of these synthetic drugs. Unfortunately, each new ban provokes the manufacture of similar chemical analogues in hopes of legally achieving the same high.

The most widely publicized and horrific bath salt-associated incident involved a man becoming cannibalistic during a drug induced psychotic break in Miami, Florida. This event occurred in late 2010, around the time bath salts first began appearing as a substance

of abuse. Toxicology screens were inconclusive for bath salts, but the man had consumed multiple unknow pills found in his stomach post-mortem. Bath salt drugs can contain one or multiple compounds that can potentially cause such mental instability. These compounds are related to the naturally occurring β-keto amphetamine parent compound, methcathinone (MCAT) (Baumann, *et al*. 2014). MCAT has been shown to have psychostimulant properties (Schechter and Glennon, 1985), but most bath salt drugs consist of a cocktail of cathinones and adulterants, including caffeine and lidocaine (Zawilska and Wojcieszak, 2013). Besides methcathinone itself, there are three main cathinones most often found in bath salts; mephedrone (4-methyl-*N*-methylcathinone, 4-CH_3 MCAT), methylone (3,4-methylenedioxy-*N*-methylcathinone), and MDPV (3,4-methylenedioxypyrovalerone). The structure of each and their relation to methcathinone can be seen below in Figure 7.

Synthetic cathinones behave by targeting monoamine transporters in the nervous system to increase extracellular monoamine concentrations within neural synapses. Synthetic cathinones, like other stimulant drugs that interact with monoamine transporters, may cause neurotransmitter rise in one of two ways. First, they can act like amphetamine by allowing greater neurotransmitter efflux, or an increased concentration of substrate to enter the synaptic cleft. Second, bath salt compounds could act like cocaine by blocking the transporters (Rothman and Baumann, 2003). The amphetamine-like mechanism produces inward currents when performing two-electrode voltage clamp. Cocaine-like drug mechanisms trigger the opposite signal, or a hyperpolarization on a two-electrode voltage clamp plot (Baumann *et al*., 2014). These results have been shown in other models as well, including HEK293 cells (Eshleman *et al*., 2013; Baumann *et al*., 2012).

A synthetic cathinone's selectivity for the dopamine transporter is a powerful estimation of that particular drug's behavioral effects. Selectivity for DAT transporters results in high locomotor stimulation, while selectivity at SERT does not (Rothman and Baumann, 2006). Methcathinone is mainly selective for DAT, while mephedrone and methylone mirror the well-known illicit drug MDMA (3,4-methylenedioxymethamphetamine, "molly", "ecstasy") by being reasonably nonselective at all monoamine transporters. Specifically, mephedrone (4-CH_3 MCAT) causes higher serotonin release but less dopamine release than methcathinone (MCAT). Cathinone analogues, that contain the same ring-structured backbone, have presented comparable nonselective results at MATs (Baumann *et al*., 2012; De Felice *et al*., 2014).

The third main bath salt compound, MDPV, exhibits selectivity unlike the other two. MDPV has been shown to be selective for DAT and norepinephrine transmitters, while prompting little effect at SERT. MDPV is 50 times more potent of a blocker at DAT than cocaine in vitro, and is 3-10 times more potent of locomotor stimulant than mephedrone or methylone (Eshelman *et al*., 2013; Baumann *et al*., 2014). MDPV is the most common compound found in the blood and urine of overdose victims, and it would not be unreasonable to assume this stems from MDPV's higher selectivity and toxicity. MDMA demonstrates nonlinear kinetics in rodents and humans, a process in which autoinhibition of its own metabolization causes higher and more sustaining blood plasma concentrations than predicted. MDPV is metabolized similarly to MDMA because of the similarities in structure and may follow nonlinear kinetics as well. Furthering this problem, some of MDPV's metabolites are also potent blockers at DAT lengthening action at the transporter even longer (Baumann *et al*., 2014). Methylone and MDPV are both self-administered in

laboratory rat models, but MDPV alone displays escalation of drug intake making its liability for abuse even higher than the other bath salt compounds (Baumann *et al*., 2014).

The four cathinone compounds listed above (methcathinone [MCAT], mephedrone [4-CH_3 MCAT], methylone, and MDPV) have either been assigned Schedule I status by the US Drug Enforcement Agency or are on temporary Schedule I status pending further evaluation. Recently, another *para*-substituted MCAT analogue flephedrone, or 4-F MCAT, has been given temporary Schedule I status due to its consistent presence in bath salts. Methedrone, or 4-OCH_3 MCAT, has not yet been scheduled but has begun appearing in drugs as well (Bonano *et al*., 2014). Preliminary data show varying potencies and efficacies at DAT and SERT for these compounds, each of which differ from MCAT by just one substituent on the benzyl ring. These variations suggest that *para*-substituted MCAT analogues might be a way for drug chemists to avoid DEA scheduled illegal compounds, but produce a compound with similar effects. Studying multiple MCAT analogue compounds with altered substituent groups could identify new drugs of abuse, and the structural elements interacting with transporters that cause behavioral and neurochemical effects.

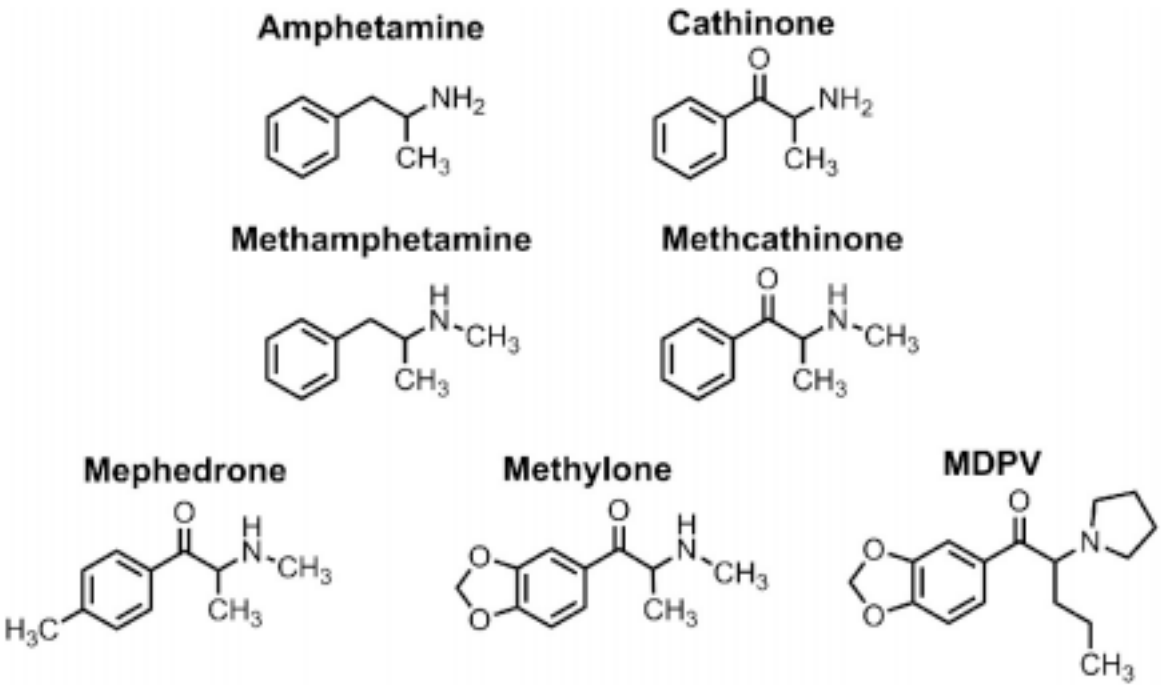

Figure 1.8 (borrowed from Baumann, *et al*., 2014): The chemical structures of the main, or parent, bath salt compounds are shown. Both mephedrone and methylone have the identical methcathinone backbone, with a different group attached to the benzyl ring. MDPV bears the cathinone backbone, but has more complicated substituents attached, which, most likely, are the reasons for its altered effects at monoamine transporters. Amphetamine and methamphetamine are also shown for comparison due to similar effects and mechanisms at transporters.

Aims of Study

As novel synthetic drug compounds continue to appear in street drug-cocktails, a better understanding is needed of the human serotonin transporter and how drugs interact with, modulate, and elicit effects at the transporter. Six new 4-*para* substituted methcathinone analogues were tested using a two-electrode voltage clamp oocyte model in order to illustrate and quantify the differences in potency and efficacy at the transporter caused by the varying substitutions.

After the raw data for each compound is acquired, the Hill equation can be used to calculate potency and maximum current. These measurements can then be correlated with other relevant factors, like electron-withdrawing capacity or lipophilicity, in order to demonstrate which specific parameters could be influencing potency and efficacy at the serotonin transporter.

Materials and Methods

3.1 Experimental Approach

Electrical currents were recorded using TEVC, mediated by hSERT expressed in *Xenopus laevis* oocytes. The oocytes were perfused with methcathinone (MCAT), flephedrone (4-F MCAT), clephedrone (4-Cl MCAT), brephedrone (4-Br MCAT), mephedrone (4-CH_3 MCAT), and methedrone (4-OCH_3 MCAT).

3.2 Human Dopamine and Serotonin Transporter RNA

A DNA linearization reaction was performed using hDAT and hSERT DNA (both amplified by VCU's DNA Core Facility). Varying amounts of DNA (10 – 30 μg) were added to Not I restriction enzyme, Buffer 3 (10x), and BSA (100x). The mixture was then diluted with ddH_2O to 30 μL total volume.

The QIAquick PCR Purification Protocol was then used to microcentrifuge the DNA. We used the Ambion mMessage Machine T7 kit to then transcribe hDAT and hSERT cRNA in the pOTV, oocyte transcription vector. The hDAT and hSERT RNA was frozen at -80 C until needed for injection.

3.3 Expression of Human Transporters in Xenopus Oocytes

Oocytes were harvested from adult *Xenopus laevis*. Anesthetization by 13% - 17% tricaine methanesulphonate solution was performed before the ovarian follicles, portions of the ovaries, were removed through a small incision on the frog's abdomen. The ovarian follicles were sliced into pieces and placed for 2 hours at room temperature in Ringer's solution with no added calcium, and with 2mg/ml collagenase type 1A. Afterward, the oocytes were rinsed with Ringer's and stored at 18 degrees Celsius.

We chose healthy stage V and VI oocytes for cRNA injection within 24 hours of oocyte harvest. Each oocyte was injected with 23.0 nL, 29.0 nL or 36.7 nL of 1μg μL^{-1} hSERT cRNA (equivalent to 23ng, 29ng, 36.7ng respectively) using Drummond Scientific Co.'s Nanoject AutoOocyteInjector. The oocytes incubated at 18 degrees Celsius for 5-10 days in Ringer's solution supplemented with 5% dialyzed horse serum, 550μg mL^{-1} sodium pyruvate, 100μg mL^{-1} streptomycin, 50μg mL^{-1} tetracycline.

Most of the setbacks encountered over the past year revolved around the oocytes and RNA injection. There did not seem to be a specific recipe or set up that guaranteed expression of hSERT in the oocytes. Each batch of oocytes was injected with a different amount of RNA; 18, 23, 27, 32, 36, or 41 nano-liters. The hSERT RNA was even diluted both 5 and 10 times before injecting for some hSERT batches. It continually appeared that the RNA was overly toxic for the oocytes and would kill them prior to transporter expression. For unknown reasons, oocytes harvested in the summer and fall are not as hardy as those harvested in the winter. Others in the lab have experienced this trend in the past and it could have contributed to the stubbornness of the oocytes these past few months.

Performing more experiments to discern approximate recipes for expression of both hSERT and hDAT would have been immensely helpful. This would eliminate hours preparing the TEVC for recording before learning that the cells were not expressing transporter. These complications limited the amount of time spent collecting data and prevented the entire data collection of all six compounds at hDAT in the time given.

3.4 Two-electrode Voltage Clamp and Analysis

A Gene Clamp 500 Voltage and Patch Clamp Amplifier and a 16-bit A/D converter were used as the voltage clamp apparatus in these experiments. Each electrode had a resistance ranging from 1 to 5 MΩ. We voltage clamped the previously injected oocytes expressing hDAT or hSERT to approximately -60mV (-55mV to -65mV range) and waited for a stable baseline to be reached while lightly perfusing buffer. The data was taken at 5 kHz and saved digitally for later analysis using 1 kHz filtering and Clampfit 10.2 software. Currents, both inward and outward, were compared with holding currents (0 to 100 nA in oocytes with -20 to -60 mV resting potentials) required for voltage clamp at -60mV.

The program *OriginLab Graphing & Analysis* was used to generate statistical plots of the data, apply the Hill or Hill1 equations, and to calculate the I_{max} and EC_{50} values.

3.5 Solutions

The oocyte incubation media consisted of: 96 mM NaCl, 0.6 mM $CaCL_2$, 2 mM KCl, 5 mM $MgCl_2$, 5 mM HEPES, 550 μg mL^{-1} Na pyruvate, 100 μg mL^{-1} streptomycin, 50 μg mL^{-1} tetracycline, and 5% horse serum, adjusted to pH 7.4 using KOH.

The extracellular two-electrode voltage clamp buffer solution consisted of (in mM): 7.5 HEPES, 1.2 Ca^{2+} gluconate, 120 NaCl, 5.4 K gluconate, and the pH was adjusted to 7.4 with KOH.

The intracellular electrode was filled with 3 M KCl.

3.6 4-*para* Methcathinone Drug Analogues

Methcathinone (MCAT) and the five analogues used in these experiments were synthesized in racemic HCL salt form by R. Glennon's lab at VCU School of Medicine using formerly published procedures: MCAT (Findlay *et al*., 1981), 4-F MCAT (Archer, 2009), 4-OCH_3 MCAT (Lespagnol and Hallot, 1954), 4-Cl MCAT (Trepanier and Sprancmanis, 1964), 4-Br MCAT (Foley and Cozzi, 2003), and 4-CH_3 MCAT (McDermott *et al*., 2011). Each compound was frozen as a 10 micro-molar solution and diluted to the appropriate concentrations when necessary for testing.

Six different compounds were tested in total. The first compound was methcathinone, the parent compound to the others, and also known by the names ephedrone or α-methylamino-propiophenone. Each of the other four analogues has a substituent group replacing methcathinone's hydrogen at the 4-*para* position on the benzyl

ring. The substituent group is often labeled as 'R' when comparing to methcathinone, as in 4-R MCAT. The second compound tested was 4-F MCAT, also known as flephedrone (4-fluoromethcathinone). Third and fourth compounds tested were 4-Cl MCAT, or clephedrone (4-chloromethcathinone), and 4-Br MCAT or brephedrone (4-bromomethcathinone). The final two compounds have a methyl group and a methoxy group attached at the 4-*para* position; fifth is 4-CH3 MCAT, or mephedrone (4-methyl methcathinone), and the sixth compound is 4-OCH3 MCAT, or methedrone (*para*-methoxymethcathinone). During testing and analysis each drug was labeled with its synthesizers initials and date, so that no bias could be introduced from previously conceived notions about the compounds.

Methcathinone was placed on the United State's federal 'Schedule I Controlled Substances' list in 1994 making it illegal and a felony to possess without permission for research. Flephedrone is currently a member of the United States' temporary Schedule 1 controlled substances list and is illegal in many other countries. Clephedrone is currently illegal in Germany, Sweden, and China but has yet to be specifically banned in the US. Brephedrone and methedrone have been outlawed in China, and mephedrone has been forbidden in many countries outside the US where the substance has repeatedly been found in recreational drugs. In 1986 the United States Congress passed the Federal Analogue Act as a part of the Controlled Substances Act. The analogue act made chemicals "substantially similar" to those compounds listed as schedule 1 or schedule 2 illegal as well, if intended for human consumption. For clarification, schedule 1 drugs are those that have a high potential for abuse, have not been approved for use in medical treatment, possess a lack of safety even under medical supervision, and have a high probability of psychological

and physical dependence. Schedule 2 drugs have a high potential for abuse, can cause severe psychological or physical dependence, but have currently accepted medical use with great restriction (dea.gov). The chemical structure of all six compounds tested can be seen on the next page with their corresponding most common names.

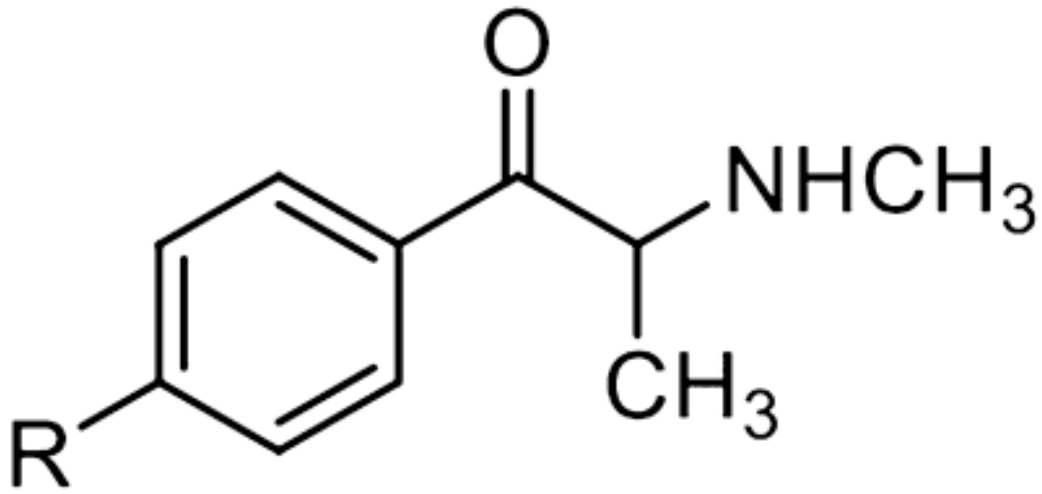

R = substituent group

-	**H**	**methcathinone**
-	**F**	**flephedrone**
-	**Cl**	**clephedrone**
-	**Br**	**brophedrone**
-	**CH_3**	**mephedrone**
-	**OCH_3**	**methedrone**

Figure 3.1 : Structure of Methcathinone and Analogues (borrowed from Bonano *et al.*, 2014). The backbone structure of methcathinone with the letter "R" representing the placement of 4-*para* substituent groups. Beneath the structure, the six different substituent groups are listed along with the common names for each. Each of the compounds can be written as 4-R MCAT instead of their common name. These compounds also can be written by describing the functional group makeup of the compound (ex: α-methylamino-propiophenone is another way of saying methcathinone), though for simplicity those names are not listed here.

Results

4.1 Two-electrode Voltage Clamp Recordings

Xenopus oocytes vary in their ability to express human RNA and in the amount of time that is required. Oocytes express the serotonin transporter (SERT) much faster than the dopamine transporter (DAT). Data was often collected within a week of injecting RNA into the oocyte, and in some cases in as little as 3 days post injection. It appeared as though the RNA was toxic for the cells after most injections. The injected cells declined in health and died much quicker than control cells injected with water, and quicker than controls that were not injected. The toxicity-caused-death often forced TEVC recordings into a very small window between the time the cells begin expressing the transporter and when the cell membrane begins breaking down and cannot hold a current to collect TEVC data.

Data collection for each drug was also complicated by the presence of a residual "shelf" most often seen in higher drug concentrations. When a shelf is present, the oocyte can no longer be used for recording because the transporter is saturated, or forced to remain open by the drug, and therefore depolarizes the resting current. The oocyte must be discarded after one reading and replaced with another oocyte because the oocyte will not return to a normal baseline.

Ideal voltage clamp command potential for oocytes is -60mV, about -10mV less than the resting membrane potential of neural cells in the human body. When testing, a range

from -55 to -65 was accepted. Generally, all data for each drug on a given transporter was collected the same day to prevent discrepancies due to health of the oocyte or differing batches of expressing injected oocytes. Example recordings from the different compounds can be seen on pages 42 and 43.

A 5μM concentration of 5-HT or DA is most commonly used as a baseline response concentration in two-electrode voltage clamp. At concentrations over 5μM, the overall response can begin to decline. This occurrence is believed to be caused by over-competition at the transporter pore, slowing down the amount of substrate and ions traveling through and decreasing the total inward current (Mager *et al*., 1994). The first recording (Fig. 4.1 A) of [10μM] methcathinone shows the smallest response of the six recordings by far, with an average response at 33.3% with [10μM]. The second recording (Fig. 4.1 B) displays flephedrone at 10μM perfusion concentration. Flephedrone's average response at this concentration is the second lowest at 61.2% average relative response for 6 recordings. Clephedrone (Fig. 4.1 E) has the third lowest average at 95.5% relative response for [10μM]. Mephedrone (Fig. 4.1 F) is fourth with an average relative response at 110.1% for 10μM concentration. Brephedrone (Fig. 4.1 C) displays the second highest response, with 112.9% relative response average at [10μM]. Methedrone (Fig. 4.1 D) clearly possesses the largest response at [10μM] with 155% shown and 142.6% average compared to the 5μM 5-HT standard.

The only compound that does not demonstrate a shelf, or potential for a shelf, after perfusion at [10μM] is methcathinone (Fig. 4.1 A). All five methcathinone analogues tested (Fig. 4.1 B-F) show a shelf after perfusion, though flephedrone and mephedrone appear to trend back towards the original baseline much faster than the other 3 analogues.

More data would be needed to quantify each compound's shelf. Therefore, it is impossible to speculate at this time as to which compound creates the largest shelf and greatest time differential before returning to baseline. It is important to note that the relative responses are given because each recording was taken using a different oocyte having an individually distinct inward current when perfused with 5μM 5-HT. So while the recordings in figure 4.1 are lined up next to each other, simply comparing them by eye is not sufficient because there is not a standard response to 5μM 5-HT perfusion. It is also worth noting that the recordings did not follow a set time frame. Some oocytes take longer than others to establish a baseline current, and therefore the amount of time before 5μM 5-HT perfusion and before drug perfusion varies for each oocyte.

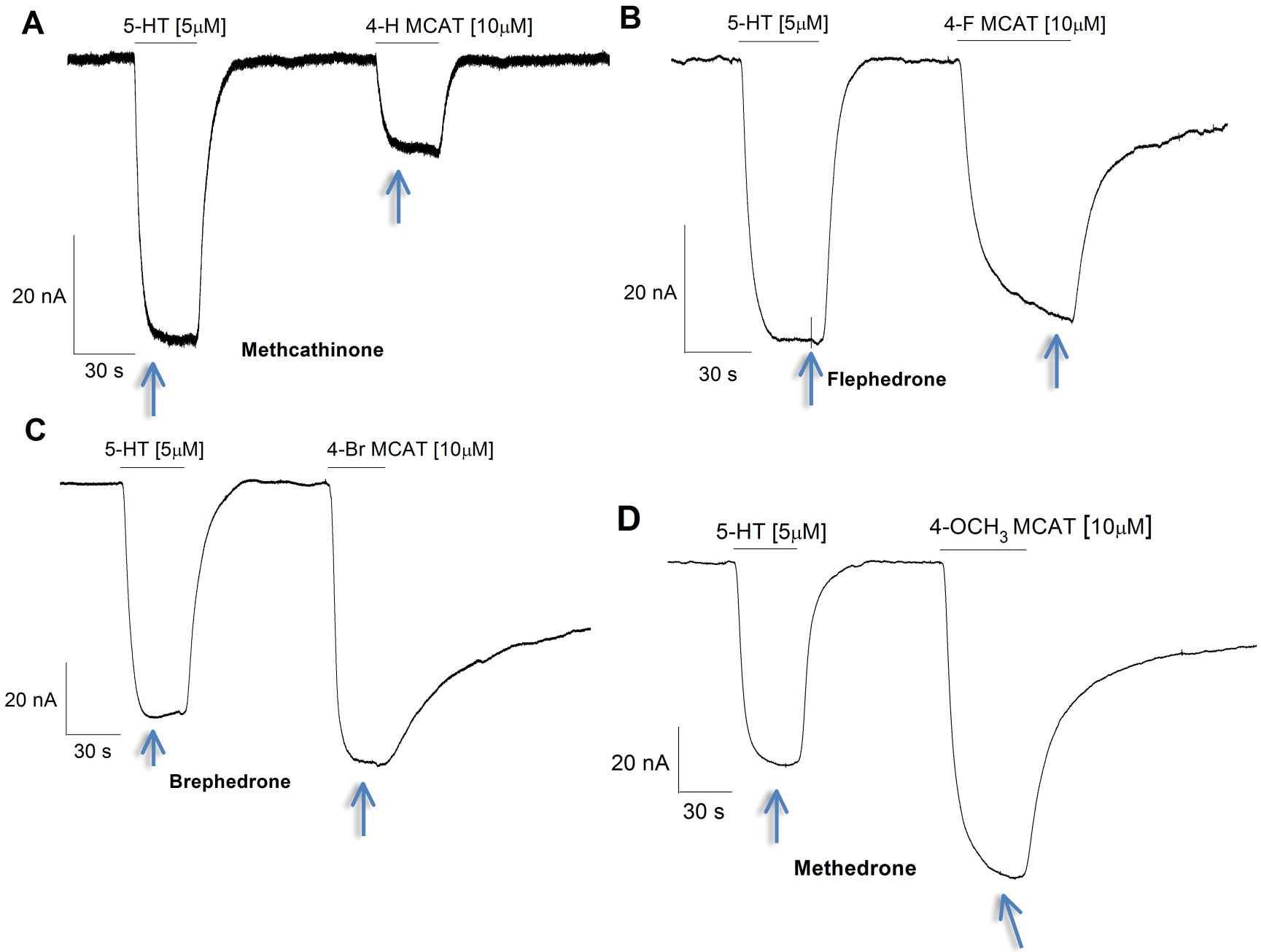

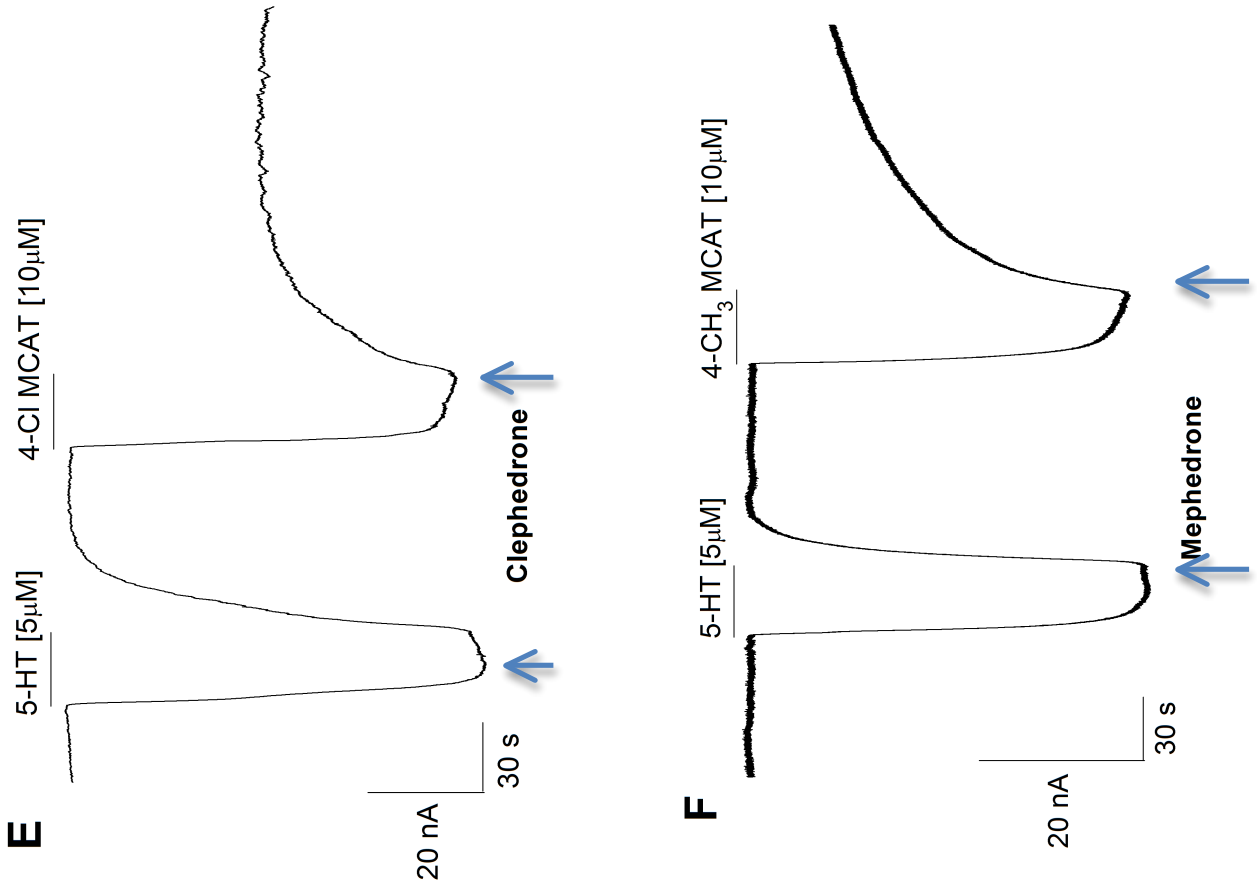

Figure 4.1 : Two-electrode voltage clamp recordings. **A**: Methcathinone recording at 10μM concentration, small relative response of 32% with no shelf present. **B**: Flephedrone recording at 10μM concentration, relative response of 93% with shelf present. **C**: Brephedrone recording at 10μM concentration, large relative response of 119% and large shelf present. **D**: Methedrone recording at 10μM concentration, large relative response of 155% and very large shelf present post brephedrone perfusion. **E**: Clephedrone recording at 10μM concentration, relative response of 92% with large shelf shown. **F**: Mephedrone recording at 10μM concentration, 94% relative response with smaller shelf slowly trending back toward the original baseline. Each arrow demarcates where resulting currents were measured.

4.2 *OriginLab* – Data Analysis and Graphics

After the two-electrode voltage clamp recordings were taken, the baseline of each graph was adjusted with the ClampFit program, if need be. When collecting the data, the sampling rate was 10kHz at an interval of 100 micro-seconds. This large amount of data was reduced by a factor of 100 and the substituted average gave the graphs shown in the previous section. After reduction and a change in baseline, the [5μM] 5-HT response was calculated from the baseline, or the point at which 5-HT was given, to the bottom of the 5-HT inward current. These nano-amp inward currents ranged in value and did not always reach a steady maximum depression. When there was not an obvious maximum depression, the nano-amp difference was calculated from baseline to the most consistent point in the bottom of the depression. The amount of inward current caused by the synthetic cathinone compounds was calculated using the same technique – from the baseline point where drug was given to the most consistent point at the bottom of the inward current. At least three calculations were taken for each drug concentration, each from a different oocyte. For most concentrations, between five and ten points were used. The calculations were entered into Microsoft Excel and a relative response was calculated by dividing the total nano-amps of drug response by the total nano-amps of 5-HT response. The calculation of relative response was required because different oocytes were used for each data point. An average of the relative responses was then calculated for each drug concentration, along with a standard deviation and standard error about the mean. For clarification, an example of Excel data entry and calculations can be seen in Table 4.2 on the following page.

hSERT					
FTS042					
File:	***5uM-5-HT (nA)***	***0.1uM-FTS024 (nA)***	***Relative Response***	***Average***	***STDEV***
14428006	*52.06*	*2.78*	*0.053399923*		
14428005	*53.5*	*1.5*	*0.028037383*		
14428004	*59.42*	*1.71*	*0.028778189*		
14428002	*37.6*	*1.98*	*0.052659574*		
14428001	*51.73*	*3.2*	*0.061859656*		
14428007	*71.69*	*1.13*	*0.01576231*	*0.040082839*	*0.01829822*
	Concentration	***Average x100***	***STDEV x100***		
	0.1	*4.00828393*	*1.8298224*		
	0.5	*5.139084075*	*3.641111815*		
	1	*7.908534475*	*3.916514355*		
	5	*43.20438348*	*4.171177312*		
	10	*89.66504423*	*16.62639977*		
	50	*80.38926255*	*3.353365103*		

Table 4.2 : Example of data entered into excel and calculations performed for each concentration of all six drug compounds. Here, example data is shown for six different TEVC calculations, all at 0.1µM concentration of flephedone (FTS-024) with their average and standard deviation (standard error about the mean not shown). Below that data, the averages for each flephedrone concentration multiplied by 100 and standard deviations multiplied by 100 are displayed (other data for flephedrone used to calculate averages not shown). The values are multiplied by 100 in order to be used as a percentage when plotting the data later in *Origin*.

The calculations of average and standard deviation (x100) for each concentration were entered into OriginLab Data Analysis program. Using this program, plots were created for each drug based on the averages and deviations. After plotting the points, the Hill equation was fitted to the plot, and the Hill equation calculated a I_{max} and a EC_{50} for each drug compound. These plots begin on the following page.

The Hill equation was developed by Archibald Hill in 1910 to quantify cooperative binding, originally to describe oxygen bound to hemoglobin. Cooperative binding is the variability (or affinity) of specific ligand binding due to the presence, or lack of, other ligands already being bound at additional sites. This is also known as allosteric control. The Hill equation is a transformation of a logistic function and the Hill equation written as a rational function for allosteric affinity calculations is:

$$I = (I_{max}[S]^n) / (K^n + [S])$$

where I is the reaction velocity, I_{max} is maximum reaction velocity, $[S]$ is substrate concentration, K is analogous to Michaelis constant (K_m) or EC_{50}, and n is the Hill coefficient – representing the degree of coopertivity. When the Hill coefficient equals 1, there is not allosteric affinity and binding of the ligand is completely independent. When the Hill coefficient is less than 1, this indicates negatively cooperative binding, which follows Michaelis-Menten kinetics and a hyperbolic plot. Positively cooperative binding occurs when the Hill coefficient exceeds 1 and follows a sigmoidal shape when plotting velocity and substrate concentration (The Biology Project, 2007).

OriginLab also offers a variation of the Hill equation, the Hill1, an offset version. Hill1 was used for 5 of 6 plots because it gave more accurate fits with the data. The Hill1 equation is: $y = [START + (END - START)] [(x^n) / (k^n + x^n)]$

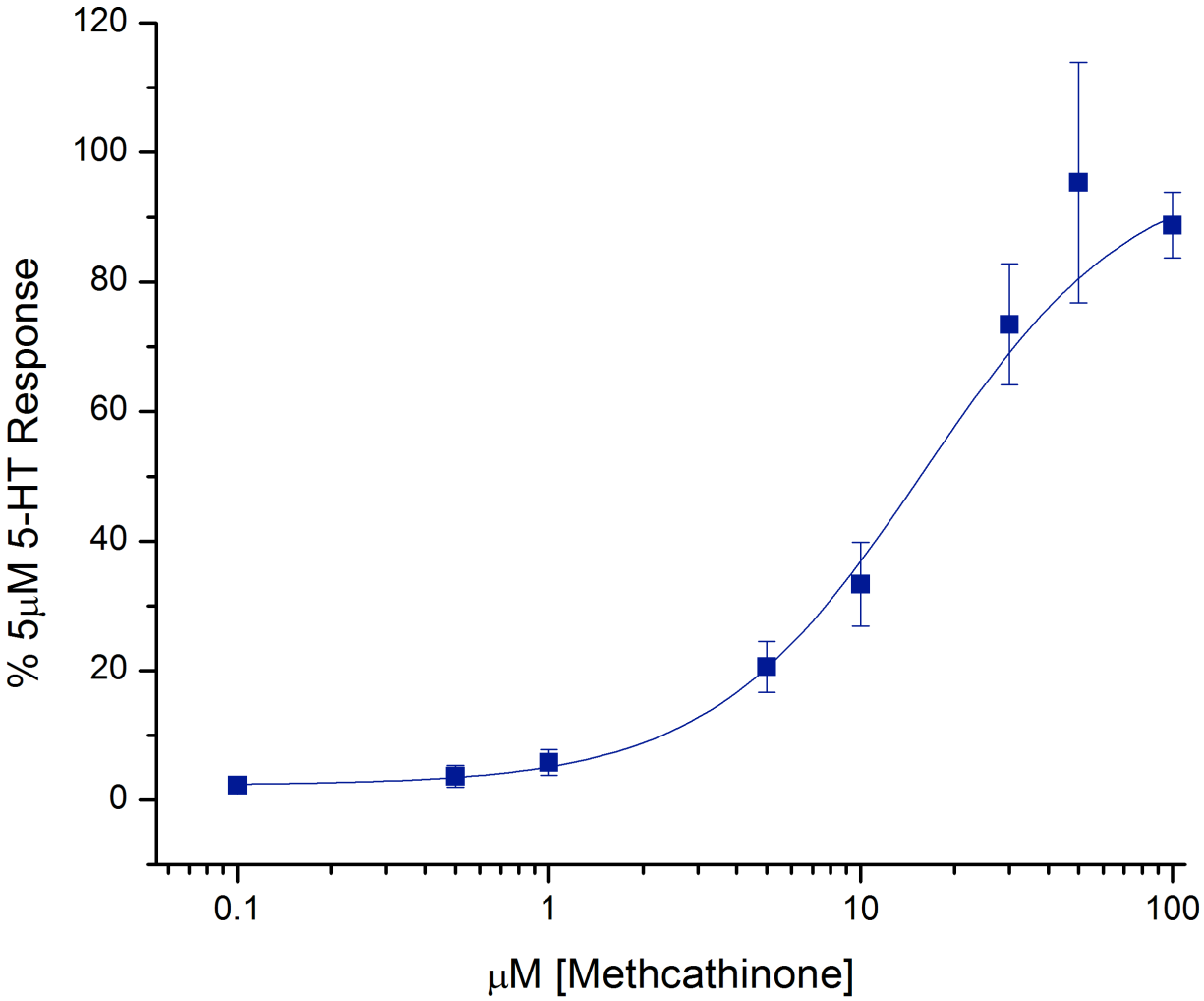

Figure 4.3 : Plot of Methcathinone's (MCAT) average relative responses at the human serotonin transporter, including error, as compared to the [5μM] 5-HT standard. Data gathered at 0.1, 0.5, 1.0, 5.0, 10.0, 30.0, 50.0, and 100.0μM-drug concentrations. A Hill1 Fit line is shown. I_{max} = 98.44% (+/- 6.37), EC_{50} = 15.73μM (+/- 3.05).

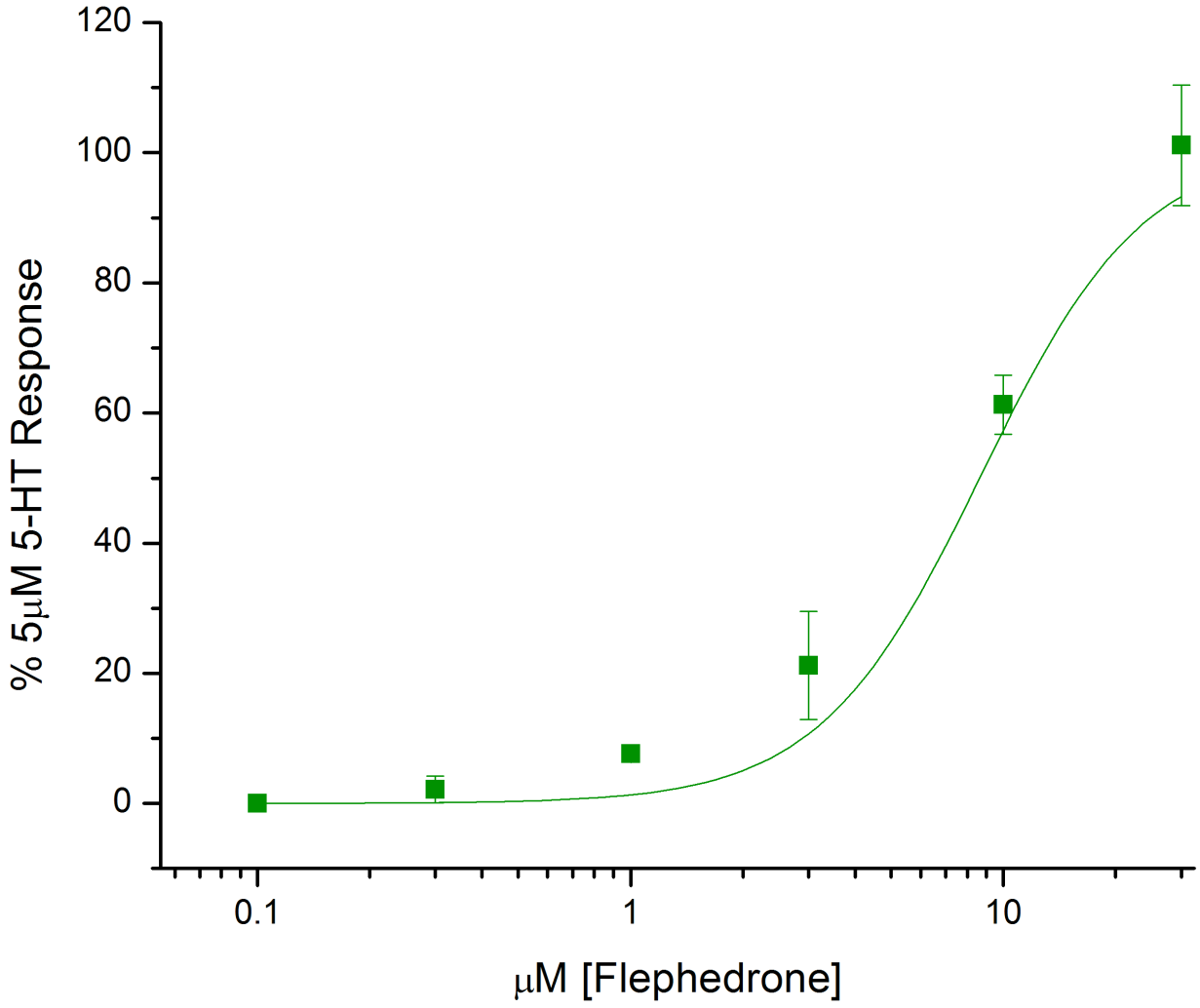

Figure 4.4 : Plot of Flephedrone's (4-F MCAT) average relative responses at the human serotonin transporter, including error, as compared to the [5μM] 5-HT standard. Data gathered at 0.1, 0.3, 1.0, 3.0, 10.0, and 30.0μM-drug concentrations. A Hill1 Fit line is shown. I_{max} = 84.55% (+/- 7.48), EC_{50} = 4.67μM (+/- 1.36).

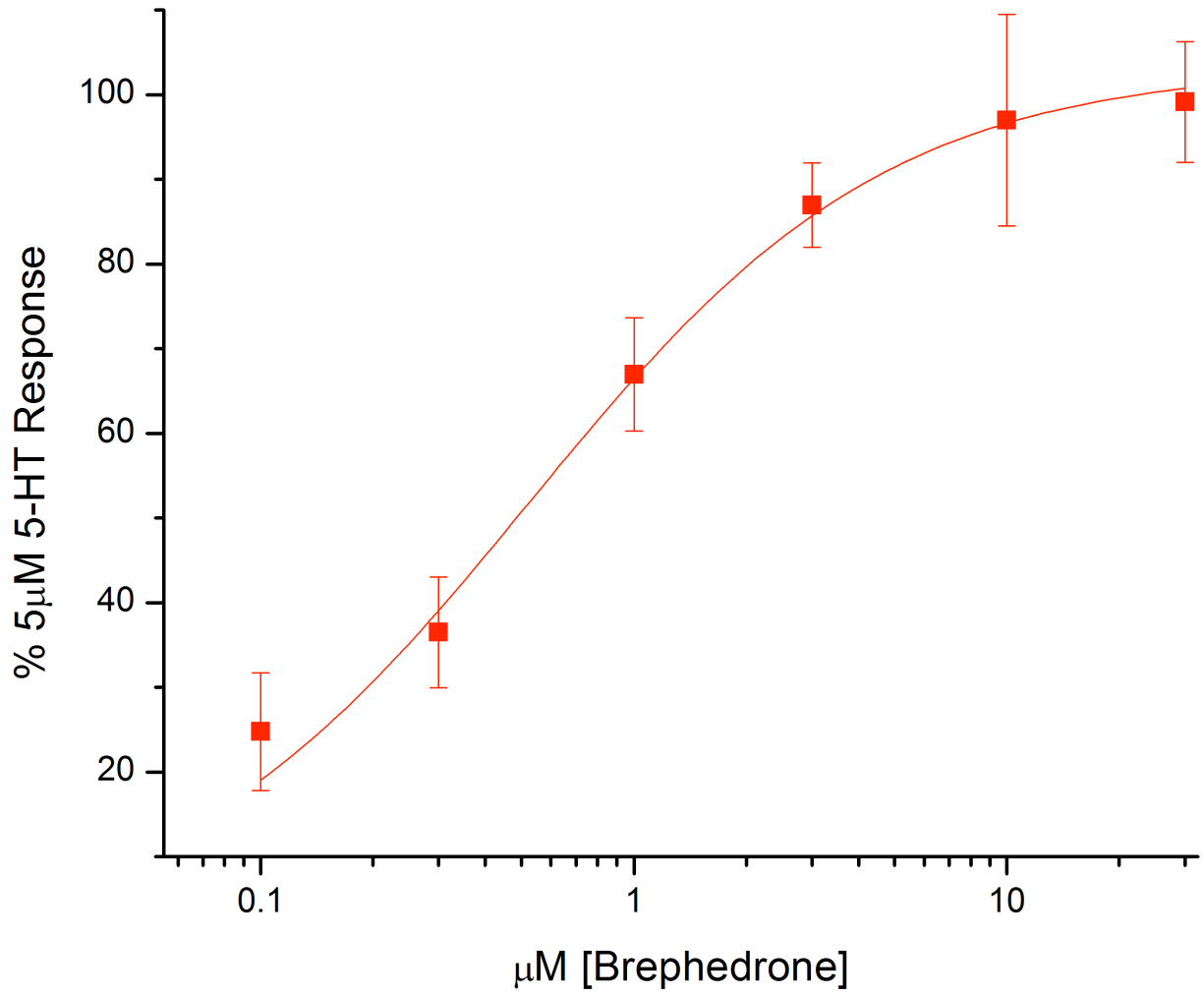

Figure 4.5 : Plot of Brephedrone's (4-Br MCAT) average relative responses at the human serotonin transporter, including error, as compared to the [5μM] 5-HT standard. Data gathered at 0.1, 0.3, 1.0, 3.0, 10.0, and 30.0μM-drug concentrations. A Hill Fit line is shown. I_{max} = 103.37% (+/- 0.57), EC_{50} = 0.52μM (+/- 0.01).

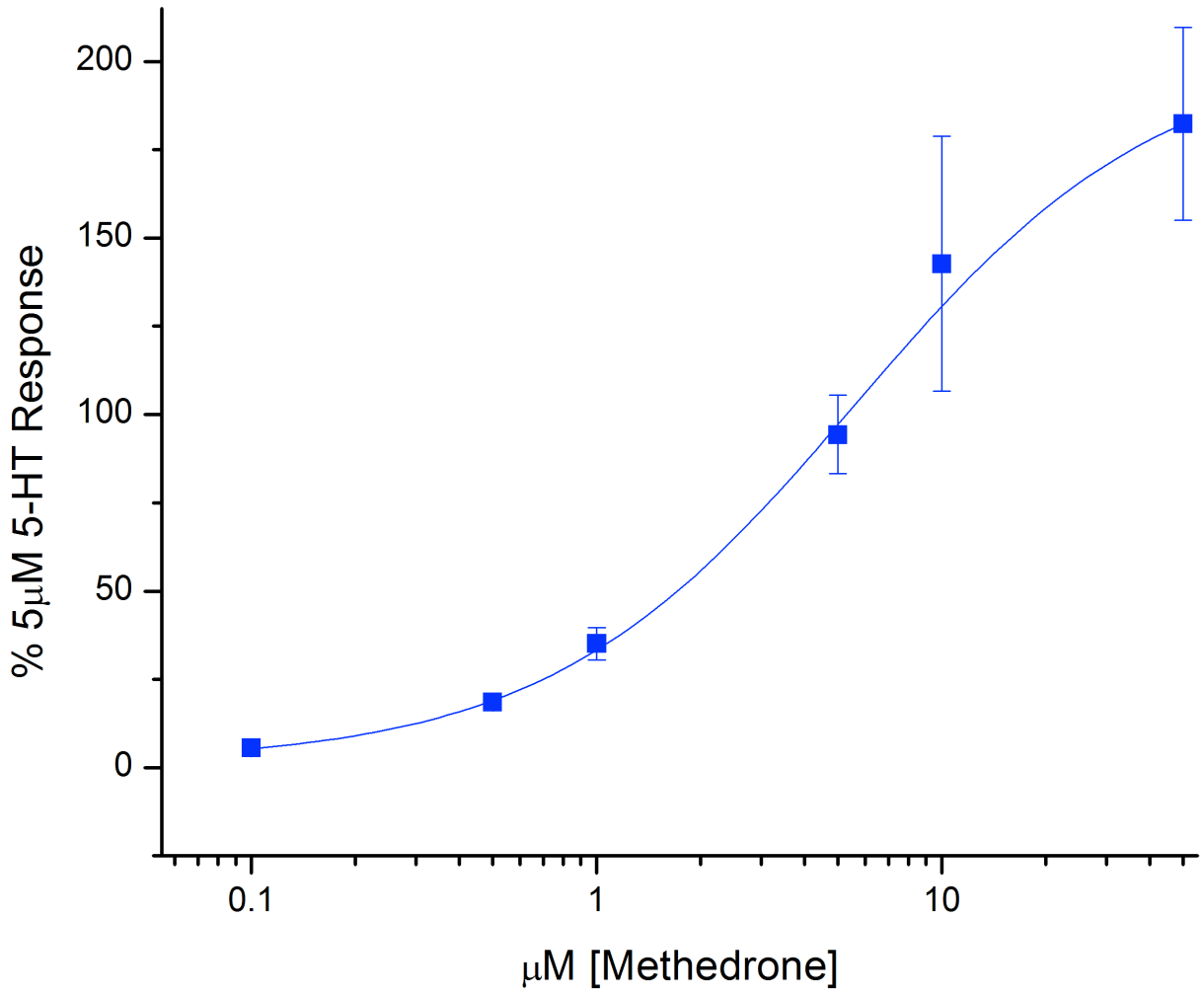

Figure 4.6 : Plot of Methedrone's (4-OCH_3 MCAT) average relative responses at the human serotonin transporter, including error, as compared to the [5μM] 5-HT standard. Data gathered at 0.1, 0.5, 1.0, 5.0, 10.0, and 50.0μM-drug concentrations. A Hill1 Fit line is shown. I_{max} = 203.39% (+/- 20.15), EC_{50} = 5.56μM (+/- 1.33).

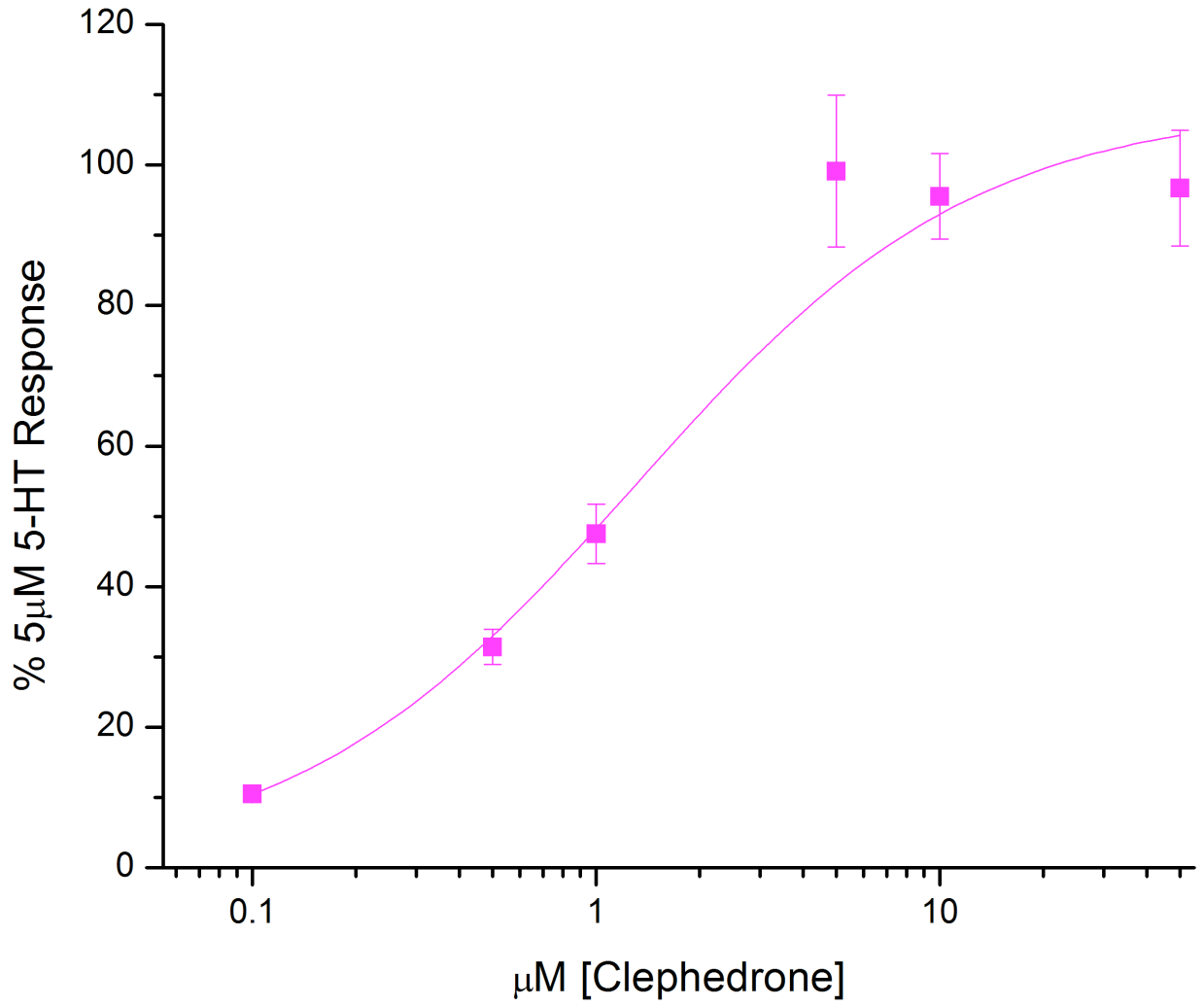

Figure 4.7 : Plot of Clephedrone's (4-Cl MCAT) average relative responses at the human serotonin transporter, including error, as compared to the [5μM] 5-HT standard. Data gathered at 0.1, 0.5, 1.0, 5.0, 10.0, and 50.0μM-drug concentrations. A Hill Fit line is shown. I_{max} = 108.46% (+/- 8.39), EC_{50} = 1.28μM (+/- 0.33).

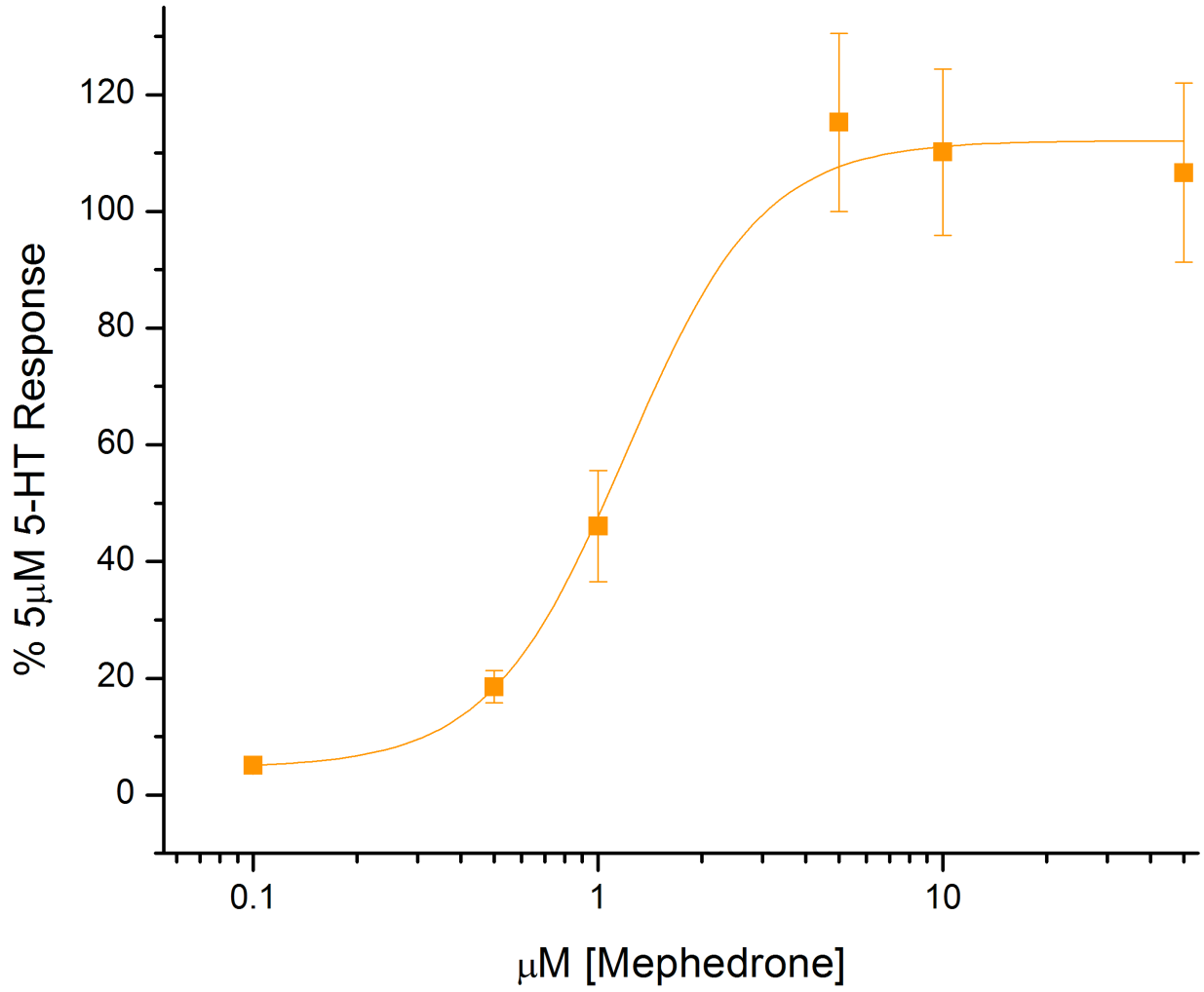

Figure 4.8 : Plot of Mephedrone's (4-CH_3 MCAT) average relative responses at the human serotonin transporter, including error, as compared to the [5μM] 5-HT standard. Data gathered at 0.1, 0.5, 1.0, 5.0, 10.0, and 50.0μM-drug concentrations. A Hill1 Fit line is shown. I_{max} = 112.12% (+/- 4.34), EC_{50} = 1.20μM (+/- 0.128).

4.3 Comparisons of Compounds

The plots shown of hSERT's response to each of the six compounds (seen on the last few pages) as compared to [5μM] 5-HT can be combined into one plot – Figure 4.9. In the Hill equation, I_{max} refers to the maximum current of the reaction. In other words, I_{max} is a measurement of how fast or efficient each drug compound can pass through the transporter alongside ions causing the inward currents seen in TEVC. Methedrone has the highest I_{max} by far, followed by the I_{max} of every other compound at about half methedrone. Exact values of I_{max} can be compared in Table 4.10 on the next page and in Figure 4.11 on the following page.

It is impossible to distinguish the EC_{50} values from the plot alone. The EC50 is the K value in the Hill equation and is also synonymous with K_M. The EC_{50} gives the effective concentration at which you reach 50% of I_{max}. In other words, it is half I_{max} or a measure of each compounds' potency. Brephedrone is the most potent compound with a EC_{50} of 0.52 followed by mephedrone at EC_{50} = 1.20. This means that for these two compounds, a 0.52μM concentration and a 1.20μM concentration cause 50% of their overall effect, respectively. Clephedrone is the third most potent with EC_{50} = 1.29, followed by flephedrone (EC_{50} = 4.67), methedrone (EC_{50} = 5.56), and finally methcathinone (EC_{50} = 15.73). These exact EC_{50} values can be compared in Table 4.10, on the following page in bar graph form on Figure 4.12, and as a scatter plot in Figure 4.13.

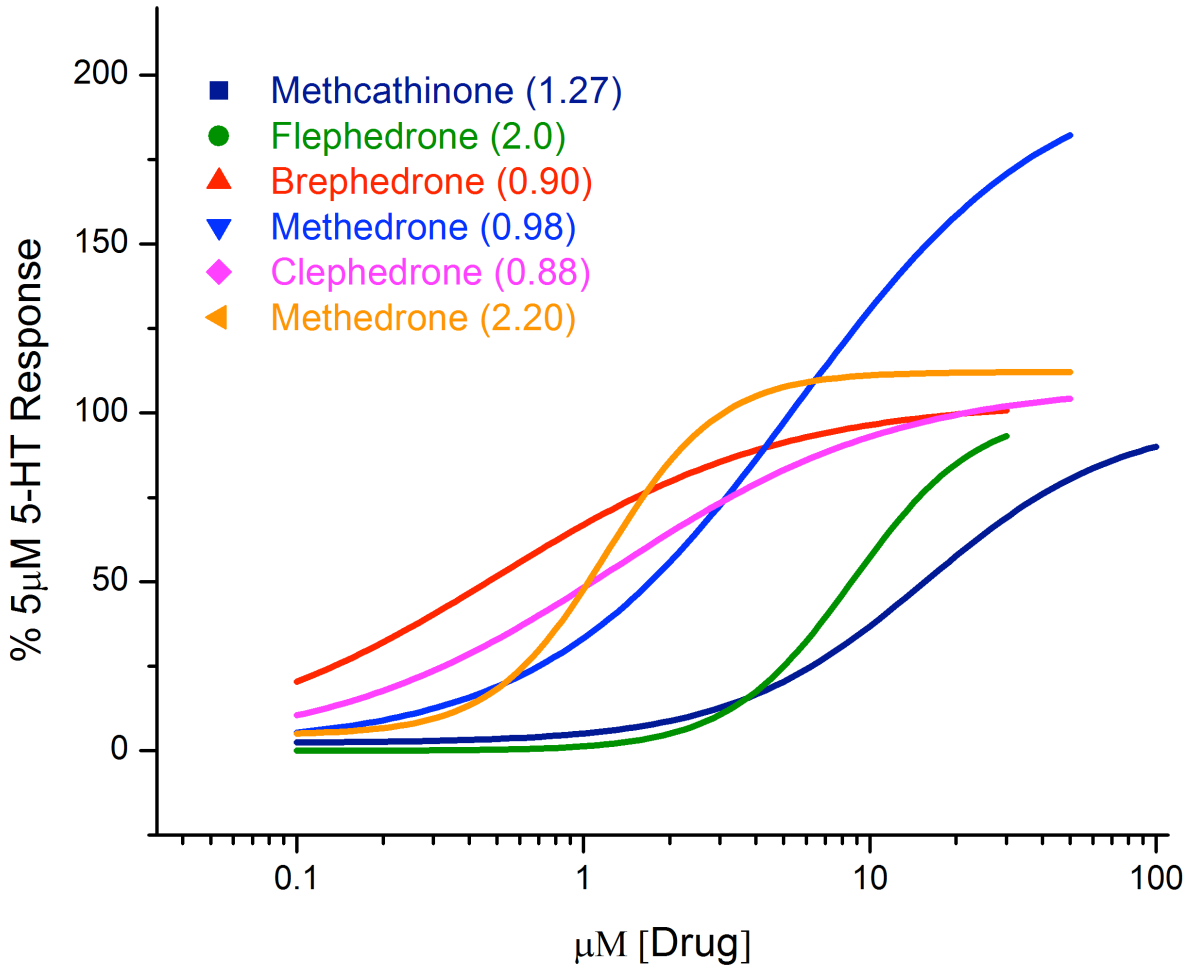

Figure 4.9 : Hill equation plots of all 6 compounds with the Hill coefficients shown in parentheses.

DRUG	I_{max}	I_{max} error	EC_{50}	EC_{50} error
Brephedrone	103.37	0.57	0.52	0.01
Mephedrone	112.12	4.34	1.2	0.128
Clephedrone	108.46	8.39	1.29	0.33
Flephedrone	84.55	7.48	4.67	1.36
Methedrone	203.39	20.15	5.56	1.33
Methcathinone	98.44	6.37	15.73	3.05

Table 4.10 : I_{max} (% of [5μM] 5-HT response) and EC_{50} (μM) for all five 4-*para* MCAT analogues and methcathinone. Compounds listed in order of potency. All errors are standard deviations from the mean.

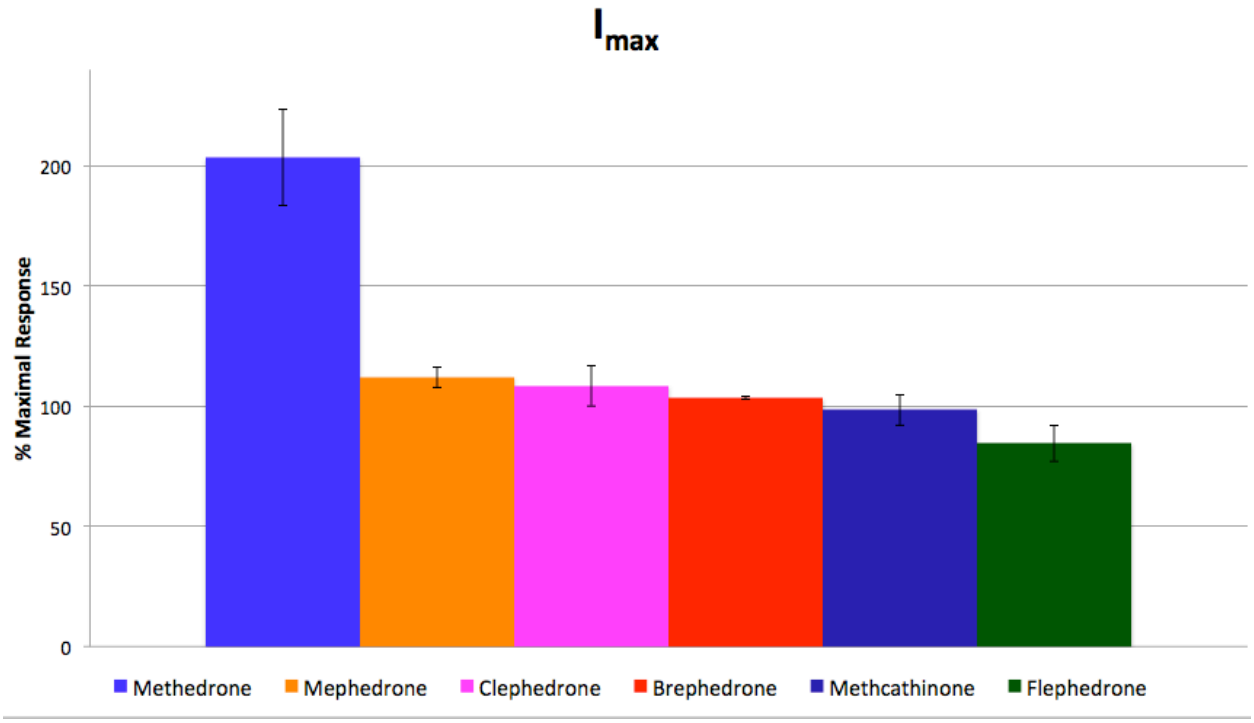

Figure 4.11 : Bar graph representation of I_{max} for all 6 compounds.

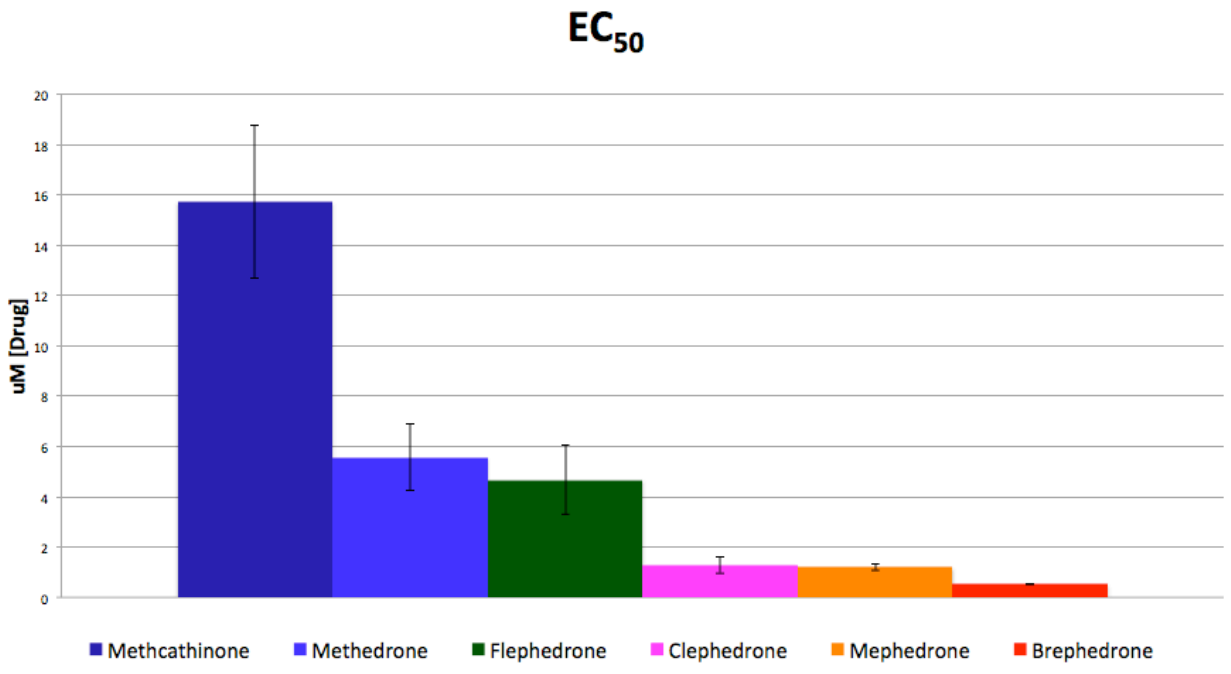

Figure 4.12 : Bar graph representation of EC_{50} for all 6 compounds.

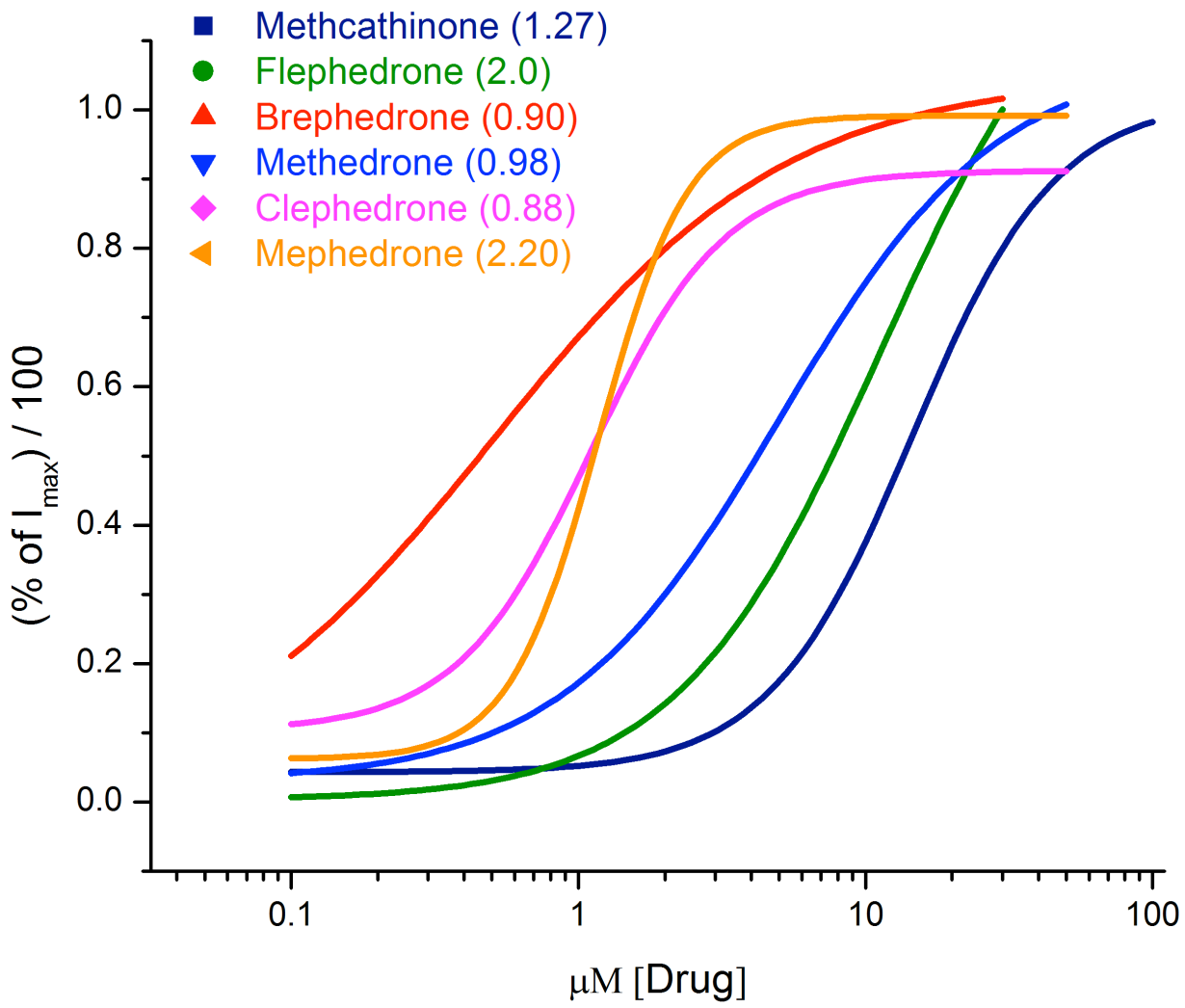

Figure 4.13: A normalized graph of all six Hill equation fits, making EC_{50} for each compound at SERT easier to visually determine. Where each line falls on the X axis, at Y value = 0.5, equals the EC_{50}. The smaller the EC_{50} value, the more potent the compound. So, for example, brephedrone's X value at Y=0.5 is smaller than clephedrone's making brephedrone the more potent compound. Hill equation coefficients are shown for each compound in parentheses.

4.4 Correlational Comparisons

The EC_{50} values calculated from concentration-effect curves in oocytes for each drug compound were first correlated with the nanomolar in-vitro release EC_{50} values from Bonano et al., 2014 and Baumann et al., 2012. The results were statistically significant, with the p value equaling 0.039 and the r value equaling 0.83, indicating a predictive relationship between the two. The correlational results can be seen in Figure 4.15.

Next, the EC_{50} oocyte values and their respective cubic angstrom volume amounts were compared. The resulting correlation gave a weak correlation between the two ($p = 0.0026$, $r = -0.56$), mainly due to the outlier methedrone (4-OCH_3 MCAT). When methedrone was excluded, it resulted in a strong correlation between the EC_{50} values and volume ($p = 0.0005$, $r = -0.992$). The results with the outlier can be seen in Figure 4.16 and the correlation without methedrone are seen in Figure 4.17.

After the previous correlations suggested that methedrone is an outlier, other correlations were performed to search for a possible explanation. First, the EC_{50} values were correlated with Taft's Steric Parameter (listed in Table 4.14), or a measure of overall steric bulk, different from the cubic angstrom values of volume used previously. This resulted in a strong and statistically significant correlation ($p = 0.003$, $r = 0.95$) and can be seen in Figure 4.18.

Next, the EC_{50} values from oocytes were correlated with the corresponding values for each 4-*para* substitution's electron withdrawing capacity. These values can be found in Table 4.14. The results from this correlation were statistically insignificant ($p = 0.377$, $r = -0.445$) and can be seen in Figure 4.19.

Values of lipophilicity for each compound were correlated with their EC_{50} values obtained from oocyte concentration-effect curves. The results were statistically significant with p = 0.004 and r = -0.933. The lipophilicity values for each compound can be found in Table 4.14 and the correlation results can be seen in Figure 4.20.

The measurements of volume do not correlate strongly with the corresponding Taft's E values, as can be seen in Figure 4.21. The correlation resulted in r = -0.65 and p = 0.16. Once again, methedrone (4-OCH_3 MCAT) appeared to be an outlier so the correlation was performed again without methedrone. The results were statistically significant (r = -0.97, p = 0.005) and can be seen in Figure 4.21 as well.

Unlike the EC_{50} values obtained from oocyte concentration curves, the EC_{50} values from Baumann *et al.* (2012) correlate strongly with Taft's E and measures of volume. The results for EC_{50} values in synaptosomes correlated with Taft's E are shown in Figure 4.22 (r = 0.88, p = 0.02) and the results for EC_{50} values in synaptosomes correlated with volume can be found in Figure 4.23 (r = -0.92, p = 0.008). All the values used can be seen in Table 4.14.

Lastly, the EC_{50} values from oocyte concentration curves were correlated with both substituent length and maximum width of the substituent. Both returned statistically insignificant correlations when methedrone (4-OCH_3 MCAT) was included. EC_{50} values correlated with length are shown in Figure 4.24 (r = -0.61, p = 0.19) and EC_{50} values correlated with maximum width are shown in Figure 4.26 (r = -0.32, p = 0.54). When methedrone was excluded, both returned strong and statistically significant correlations. Figure 4.25 displays the correlation between EC_{50} values and substituent length, without methdrone (r = -0.96, p = 0.01). The correlation between EC_{50} values and substituent

maximum width, excluding methedrone, can be seen in Figure 4.27 (r = -0.95, p = 0.01). The values for substituent length and width were borrowed from the Sakloth *et al.* (2014) paper and can be found below in Table 4.14.

Drug	EC50 - Oocytes	EC50 - Synaptosomes	Volume	Taft's E	EWC	Lipophilicity	Length	Max Width
Brephedrone	0.52	60.2	169.43	0.08	0.23	0.86	3.83	1.95
Mephedrone	1.2	118	166.89	0	-0.17	0.56	3	2.04
Clephedrone	1.29	144	164.43	0.27	0.23	0.71	3.52	1.8
Flephedrone	4.67	1290	153.78	0.78	0.06	0.14	2.65	1.35
Methedrone	5.56	120	175.01	0.69	-0.27	-0.02	3.98	3.07
Methcathinone	15.73	3860	150.36	1.24	0	0	2.06	1

Table 4.14: Values used in each correlational comparison. The EC_{50} values in oocytes are measured in micromolar amounts. EC_{50} values in synaptosomes are nanomolar (Bonano *et al*., 2014, Baumann *et al*., 2012) and volume is cubic angstroms (Sakloth, *et al*. 2015). Taft's values are a measure of functional steric bulk, EWC is short for 'electron-withdrawing capacity', and the lipophilicity of each compound is also shown.. (Sakloth, *et al*. 2015). Physochemical parameters (Taft's, EWC, Lipophilicity) borrowed from Wolff, 1980. Finally, the length of substituent (Å), and maximum width of substituent (Å) for each compound are also listed (Sakloth, *et al*. 2015).

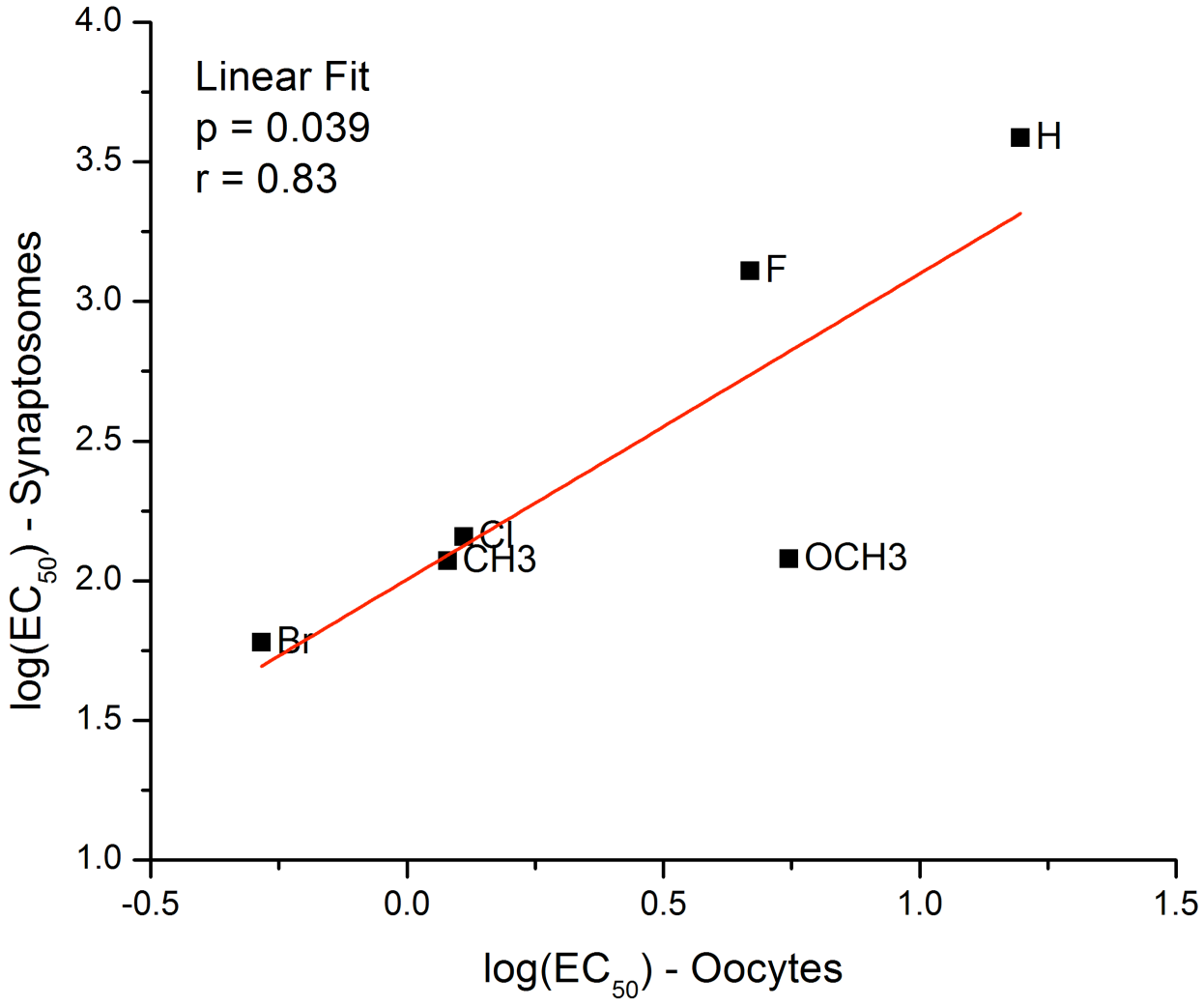

Figure 4.15: LogEC_{50} values from concentration-effect curves in oocytes correlated with the logEC_{50} values from Bonano et al., 2014 and Baumann et al., 2012, found in Table 4.14.

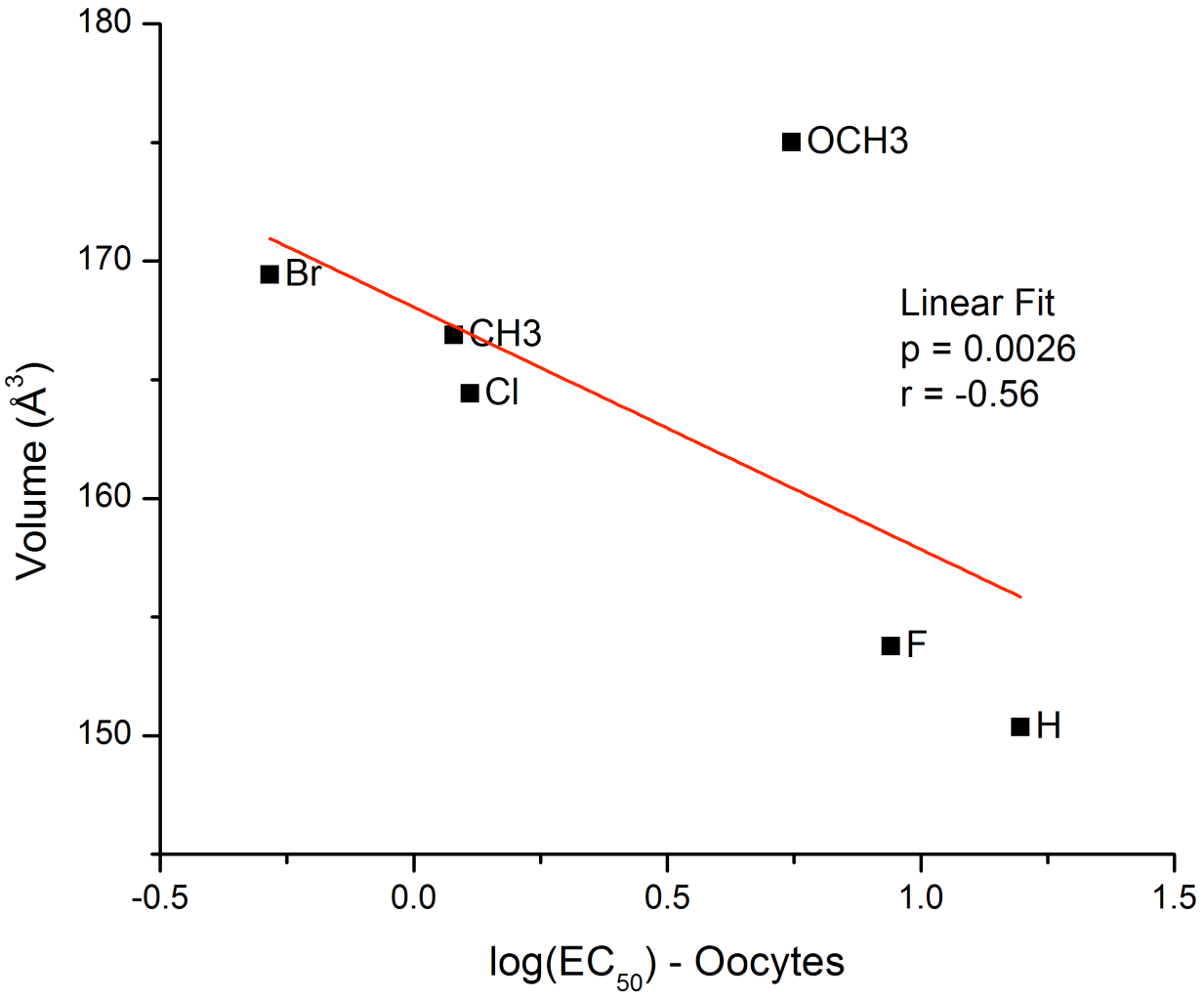

Figure 4.16: Correlational analysis of EC_{50} values obtained from oocyte concentration-effect curves including methedrone (4-OCH_3 MCAT). Results are statistically significant but with a very weak correlation. Volume values for each compound can be found in Table 4.14.

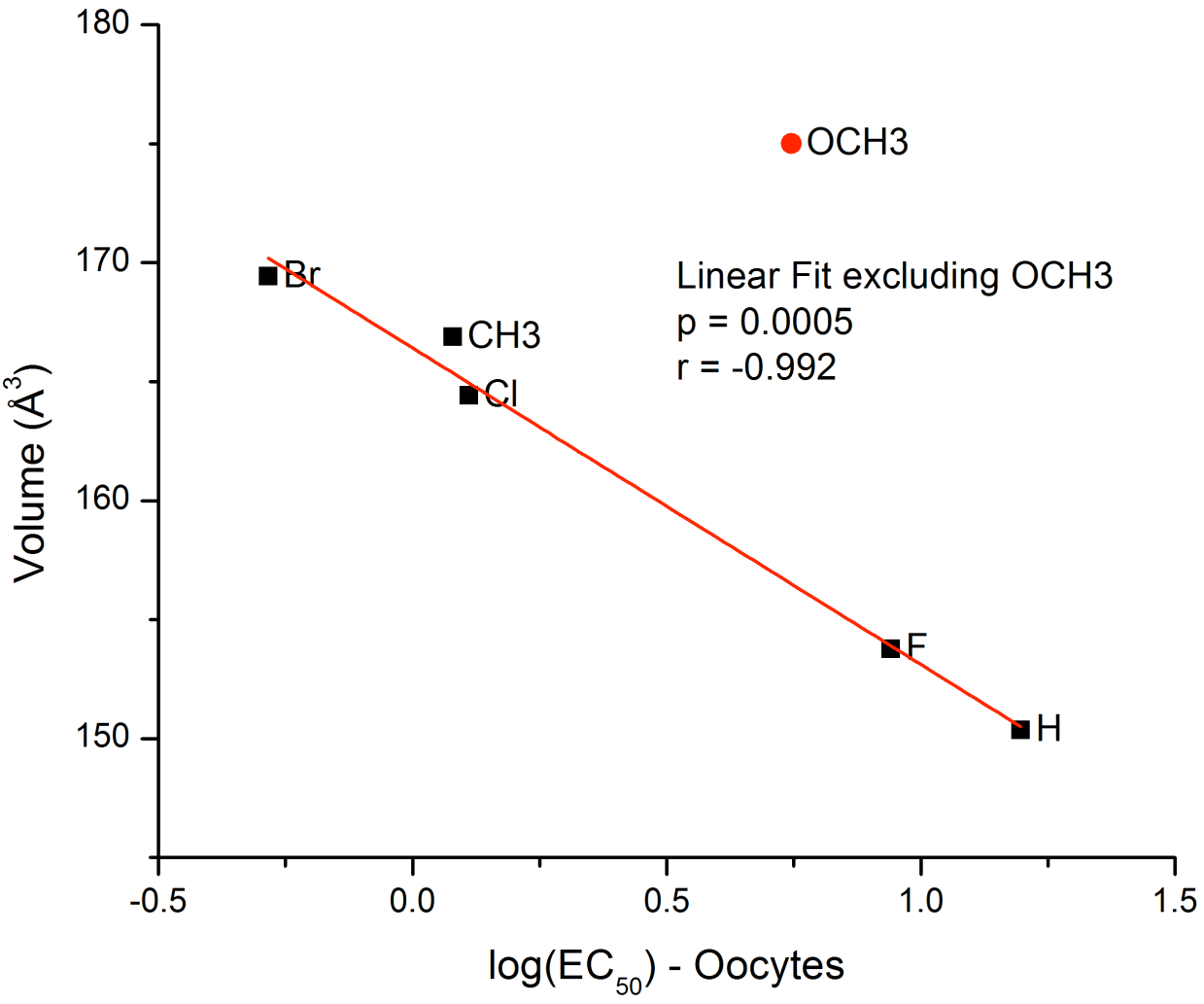

Figure 4.17: Correlational analysis of EC_{50} values obtained from oocyte concentration-effect curves and respective values of volume for each compound, excluding methedrone (4-OCH_3 MCAT) shown here in red. Results are statistically significant, with a very strong correlation suggesting that methedrone is an outlier. Volume values for each compound can be found in Table 4.14.

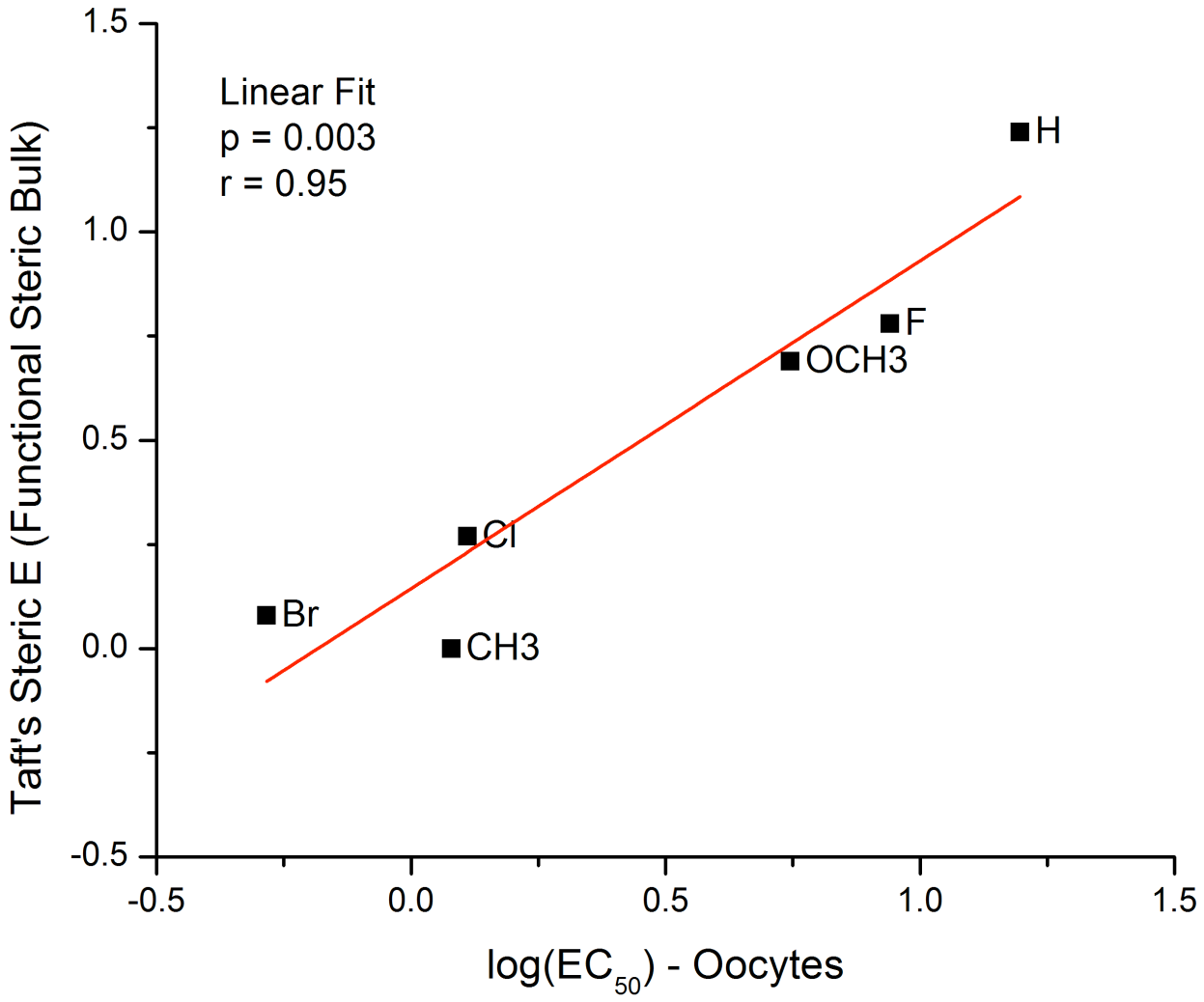

Figure 4.18: Correlational analysis of EC_{50} values obtained from oocyte concentration-effect curves and Taft's Steric E values, or a measure functional steric bulk. Taft's values for each compound can be found in Table 4.14.

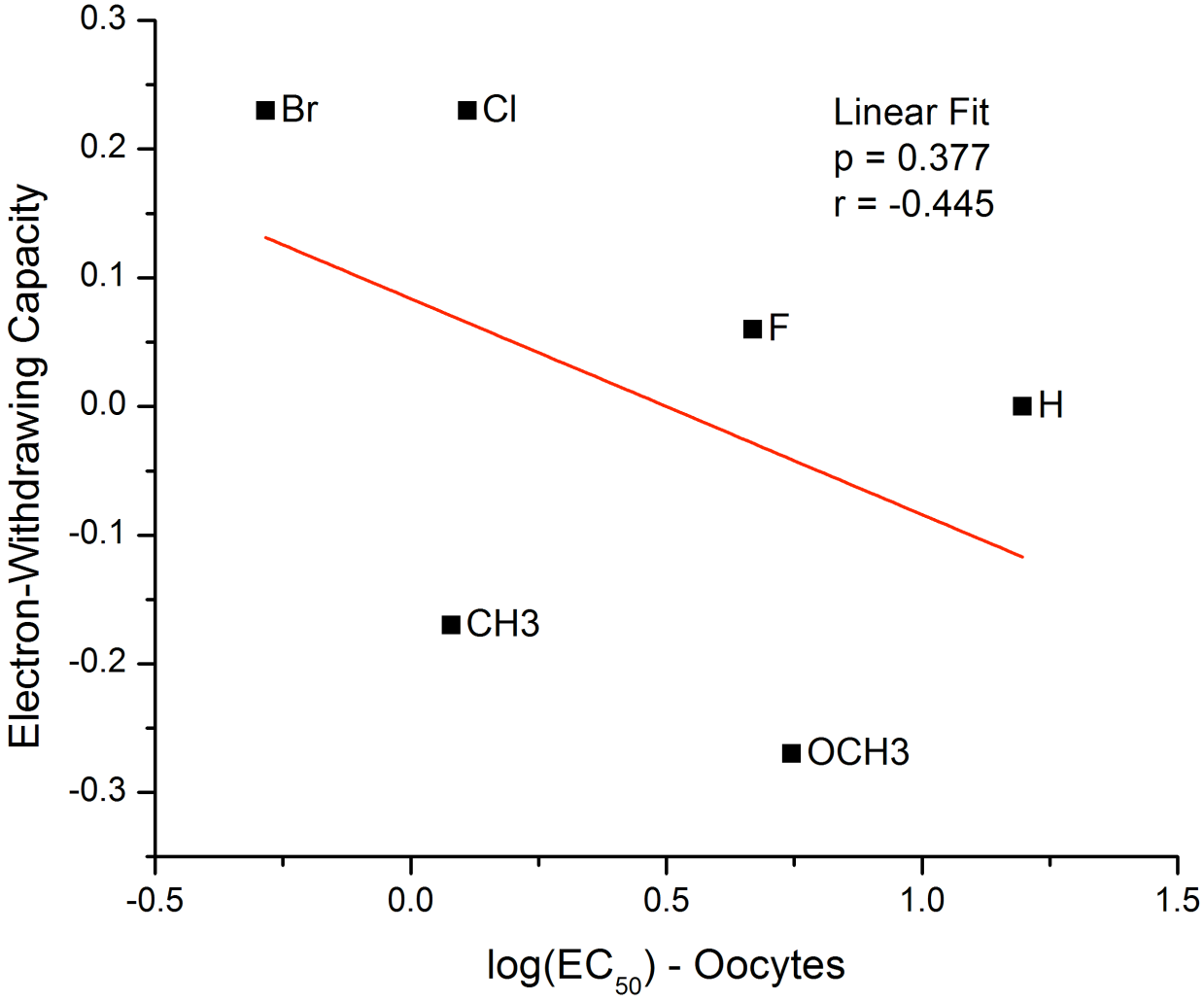

Figure 4.19: Correlational analysis of EC_{50} values obtained from oocyte concentration-effect curves and Electron-Withdrawing Capacity (EWC) values. EWC values for each compound can be found in Table 4.14. This correlation is statistically insignificant, but if we exclude 4-CH_3 MCAT and 4-OCH_3 MCAT then the results are statistically significant (r = -0.96, p = 0.04).

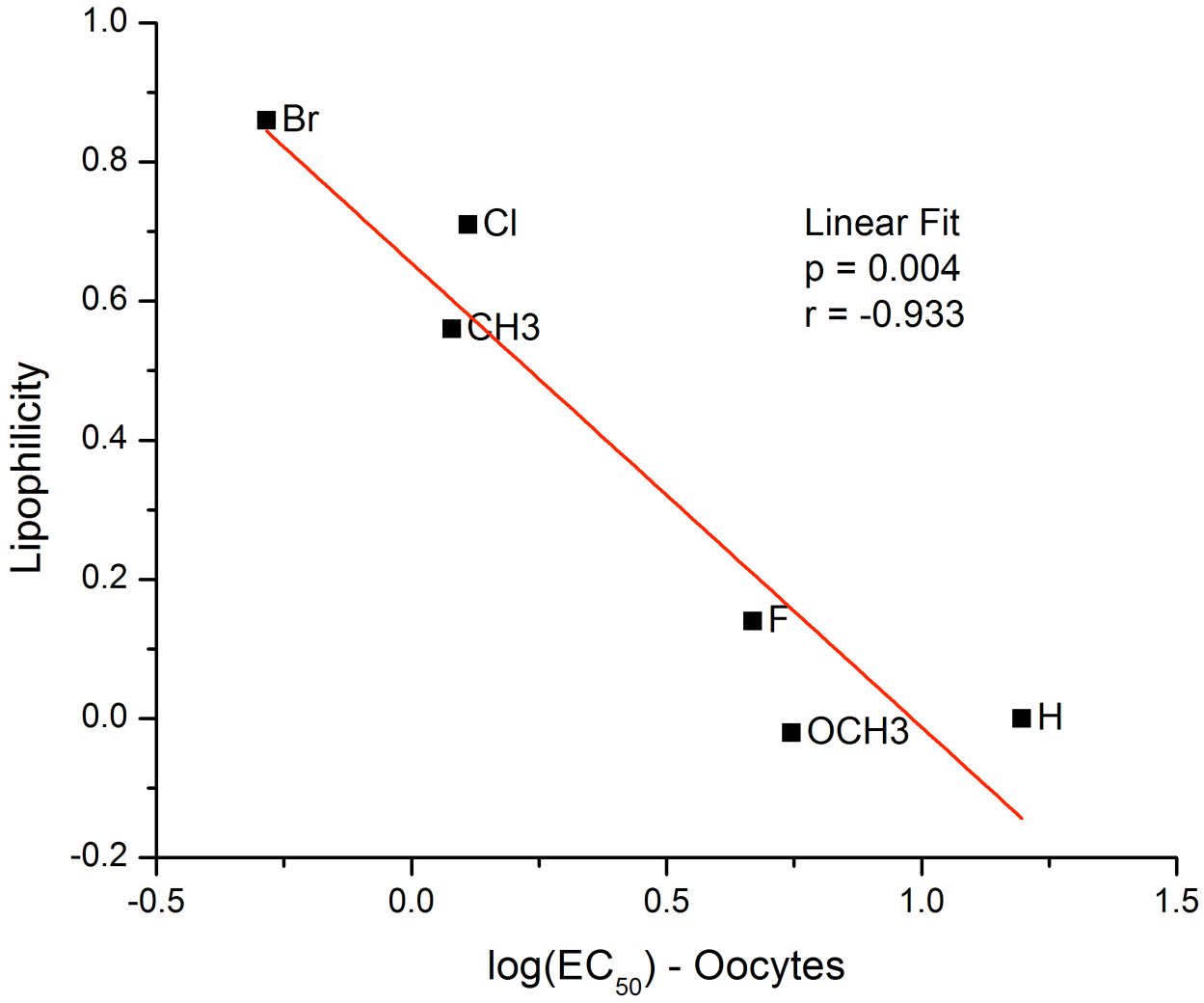

Figure 4.20: Correlational analysis of EC_{50} values obtained from oocyte concentration-effect curves and lipophilicity values. Lipophilicity values for each compound can be found in Table 4.14.

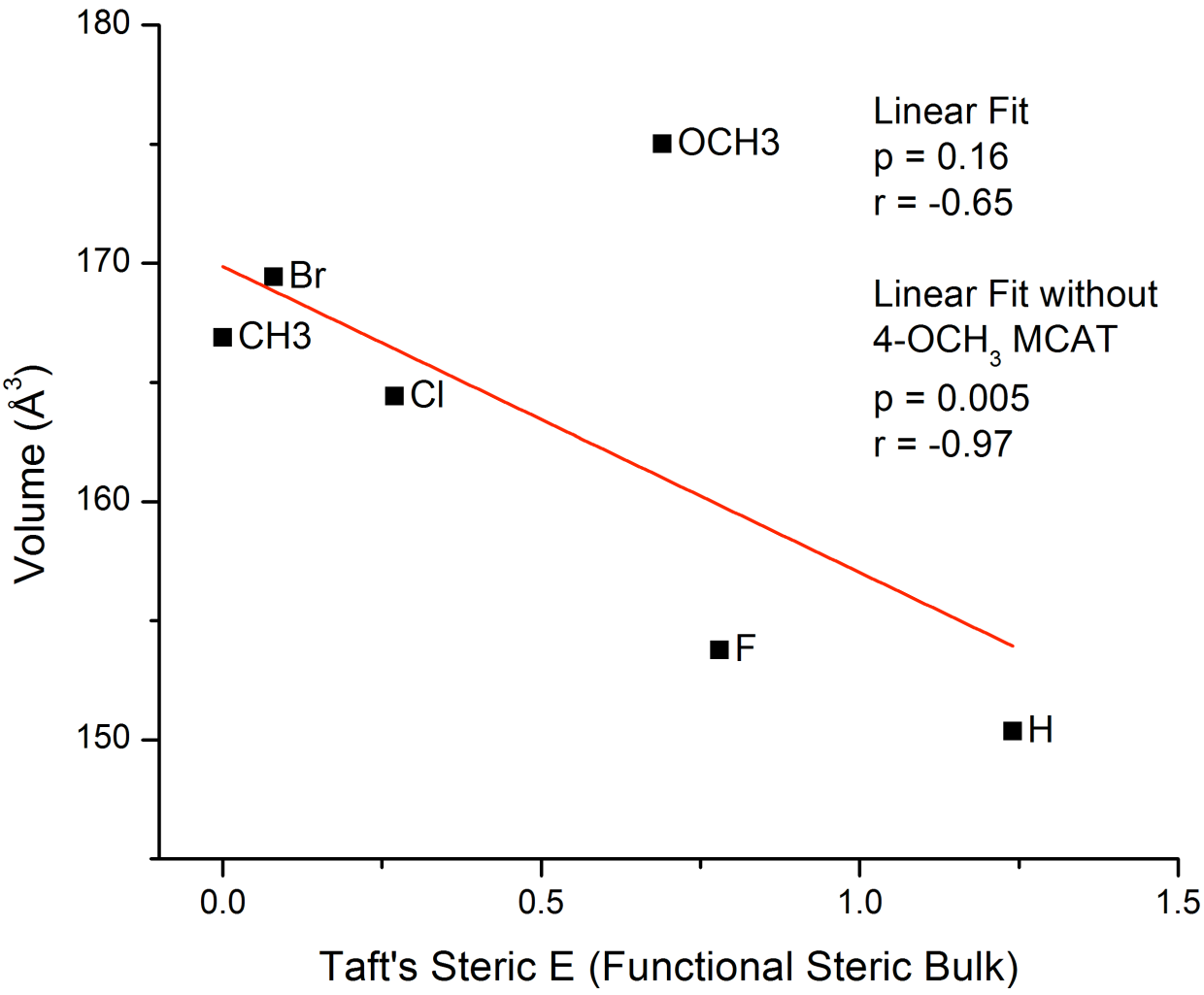

Figure 4.21: Correlation between Taft's Steric E and the volume of each methcathinone analog. All values can be found in Table 4.14. The correlation between Taft's and Volume is weak and statistically insignificant, r = =0.65 and p = -0.16. When methedrone (4-OCH_3 MCAT) is excluded, r = -0.97 and p = 0.005, suggesting that particular point is an outlier.

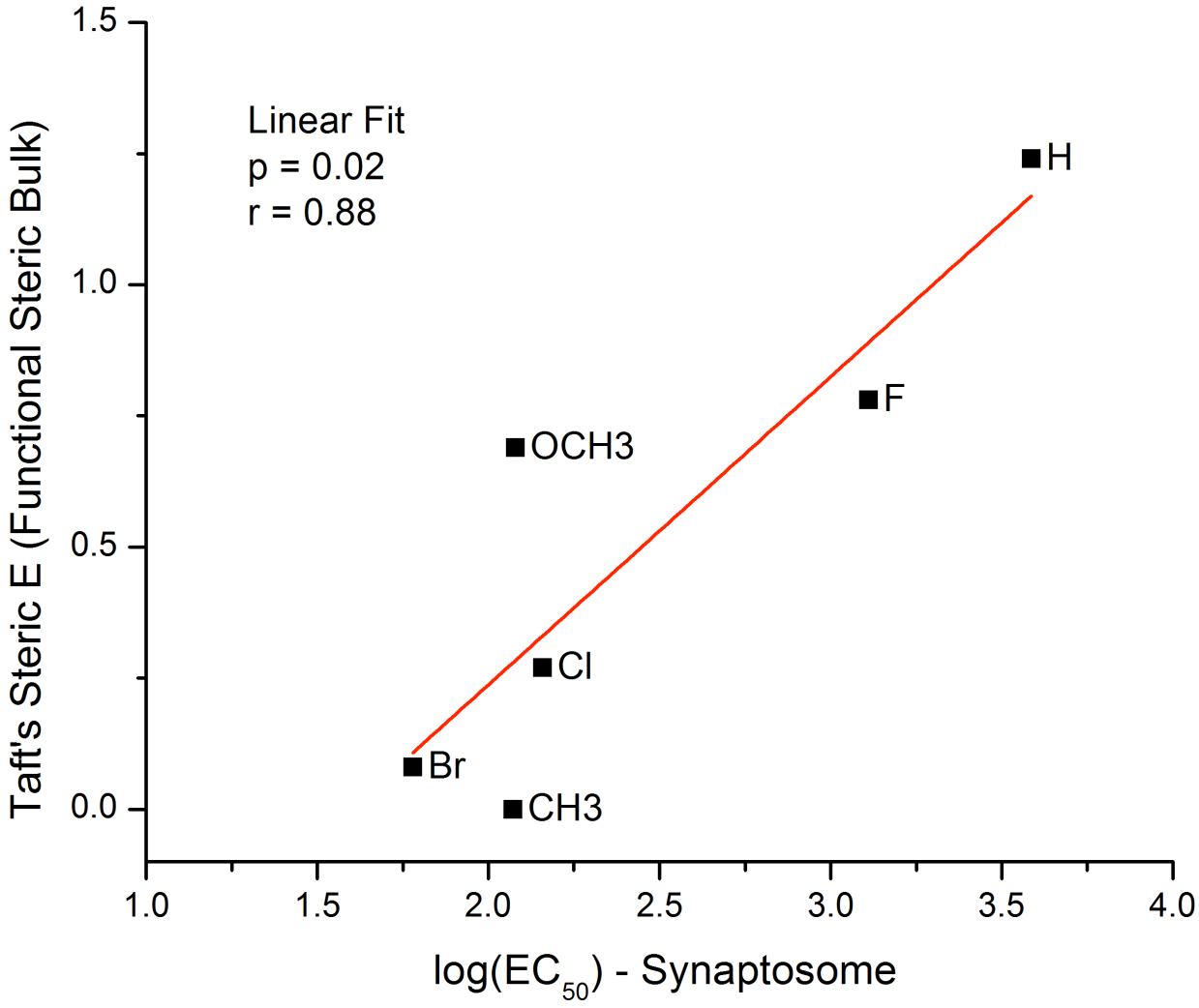

Figure 4.22: Correlational analysis between all six EC_{50} values in synaptosomes (Baumann *et al.*, 2012) and Taft's Steric E (Bonano *et al.*, 2014). The result is statistically significant, with an r value of 0.88 and a p value of 0.02. All values can be found in Table 4.14.

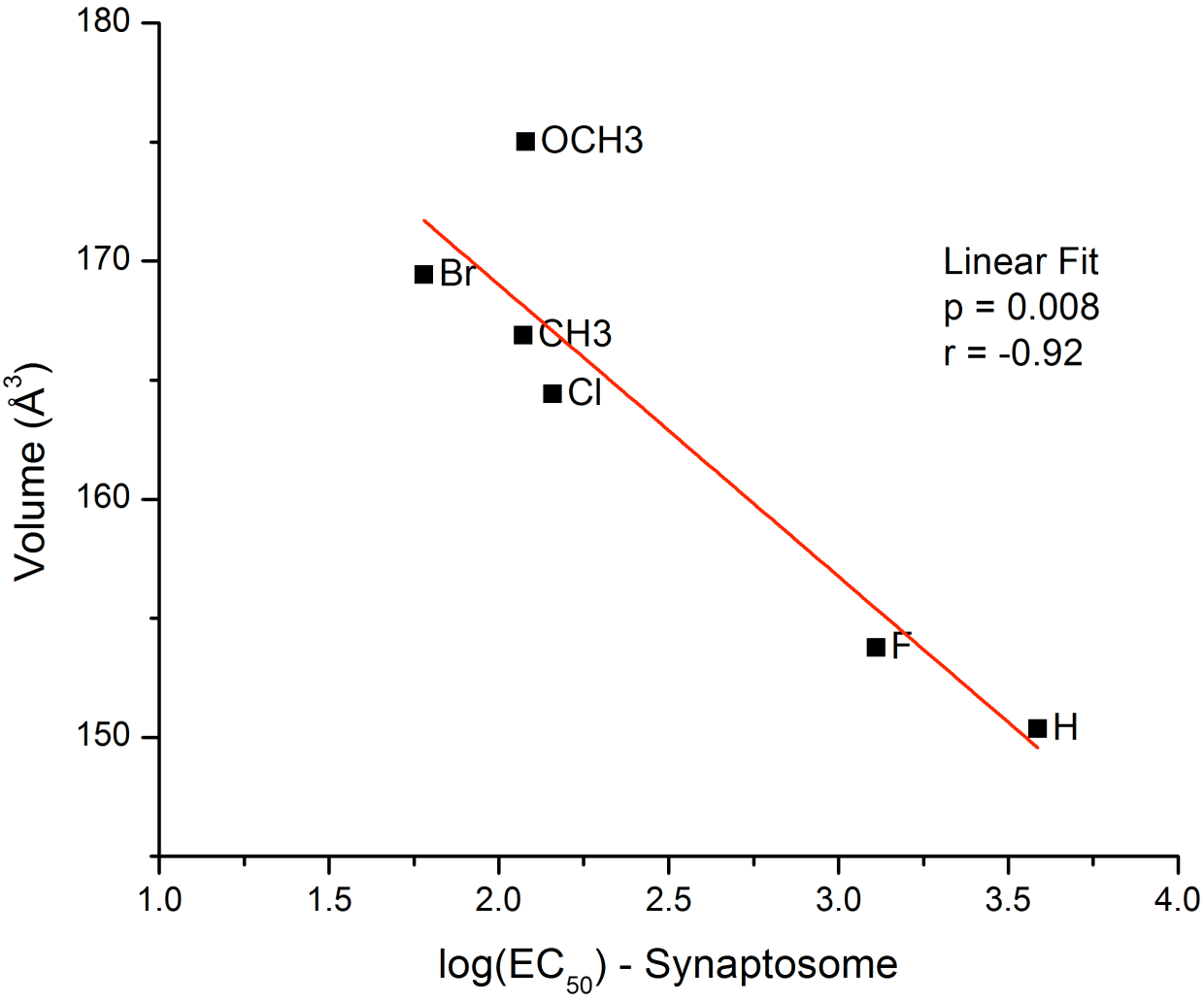

Figure 4.23: Correlational analysis between all six EC_{50} values in synaptosomes (Baumann *et al.*, 2012) and the volume of each corresponding compound. The correlation is statistically significant, r = -0.92 and p = 0.008. All the values can be found in Table 4.14.

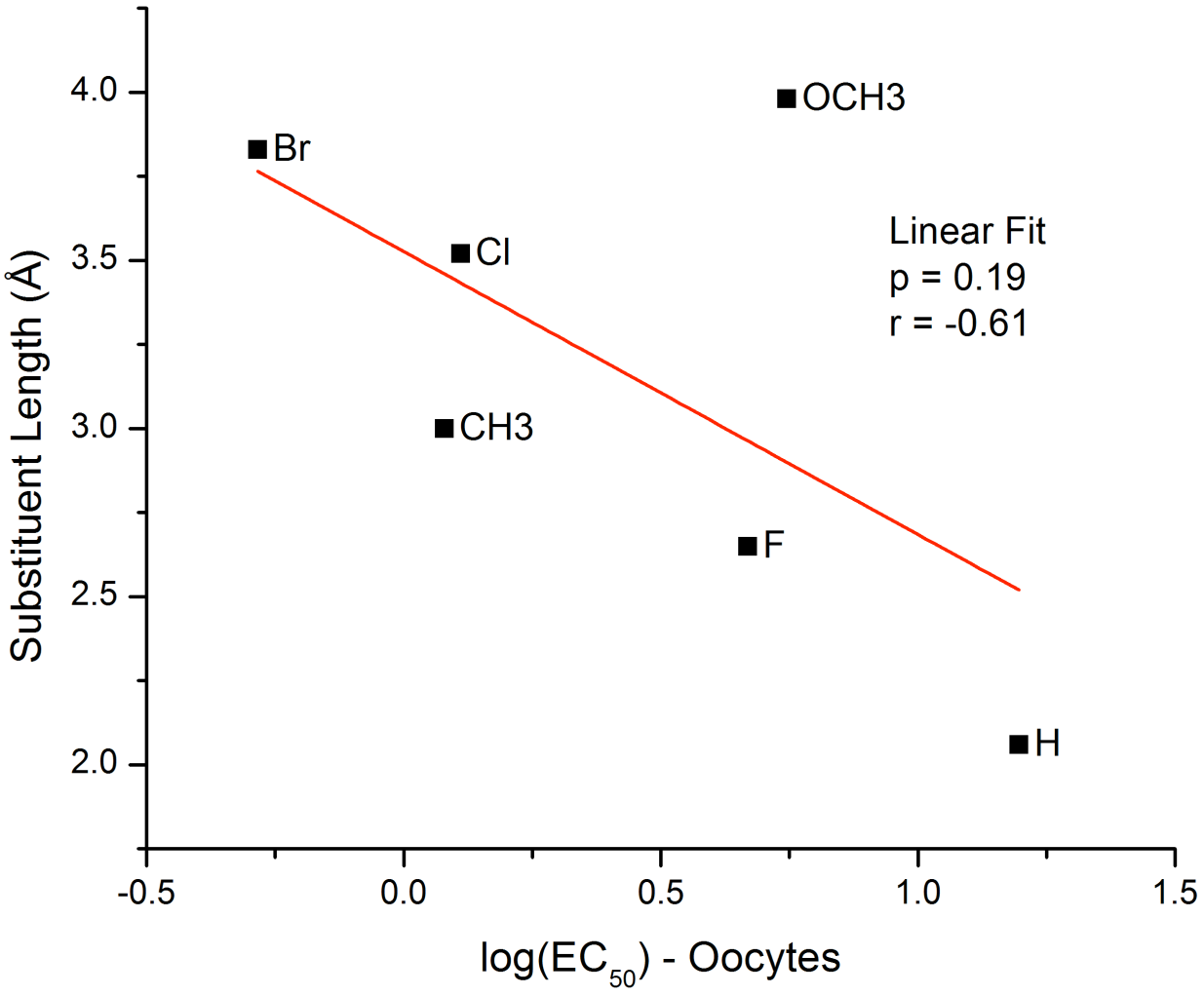

Figure 4.24: The EC_{50} values from concentration curves in oocytes correlated with the length of each substituent, in angstroms. The substituent length values can be found, along with the EC_{50} values, in Table 4.14. The correlation gave a statistically insignificant result, r = -0.61 and p = 0.19.

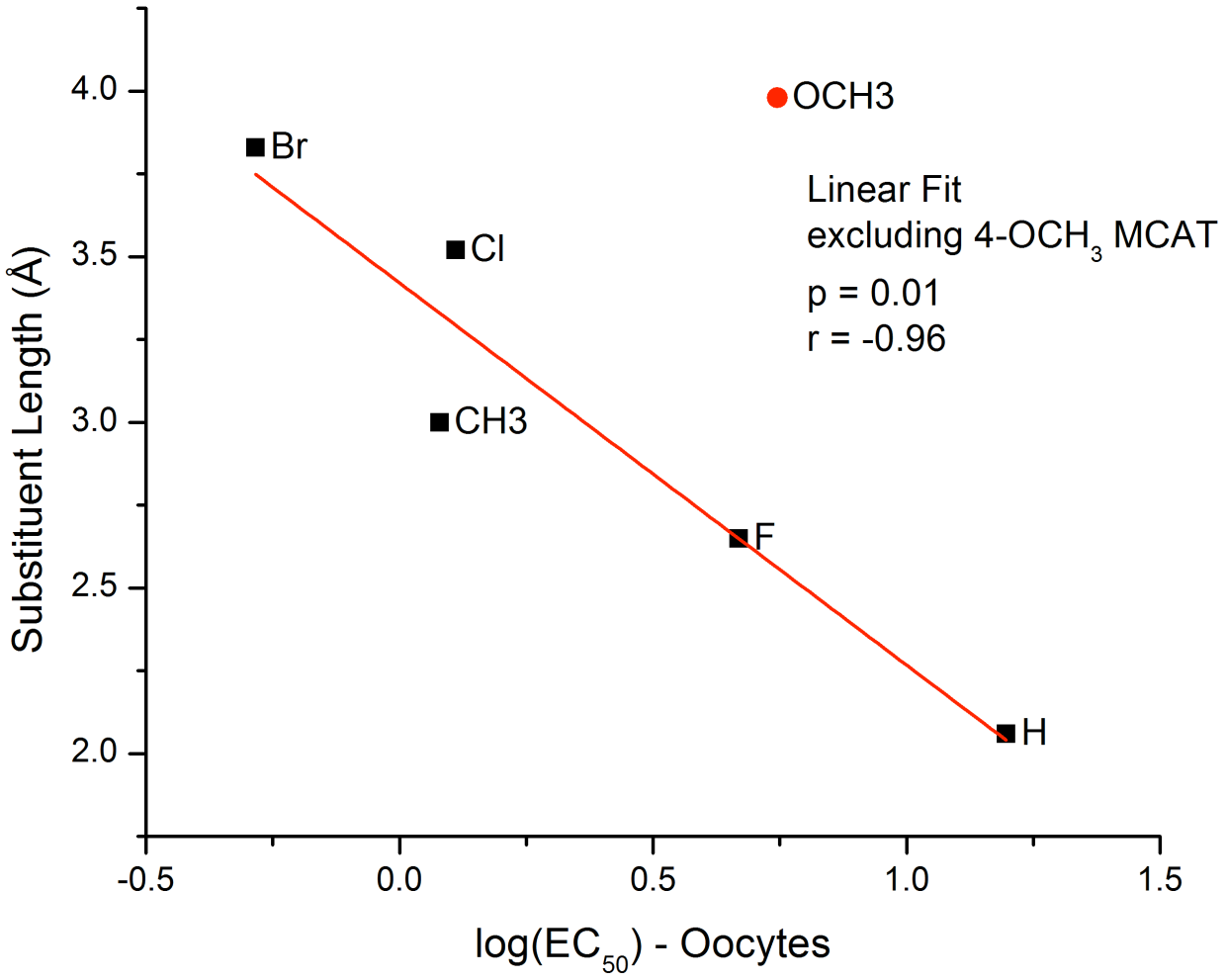

Figure 4.25: Excluding methedrone (4-OCH_3 MCAT), the EC_{50} values from concentration curves in oocytes correlated with the length of each substituent. The substituent length values can be found, along with the EC_{50} values, in Table 4.14. Unlike the previous correlation (with methedrone included), the results were statistically significant – r = -0.96 and p = 0.01.

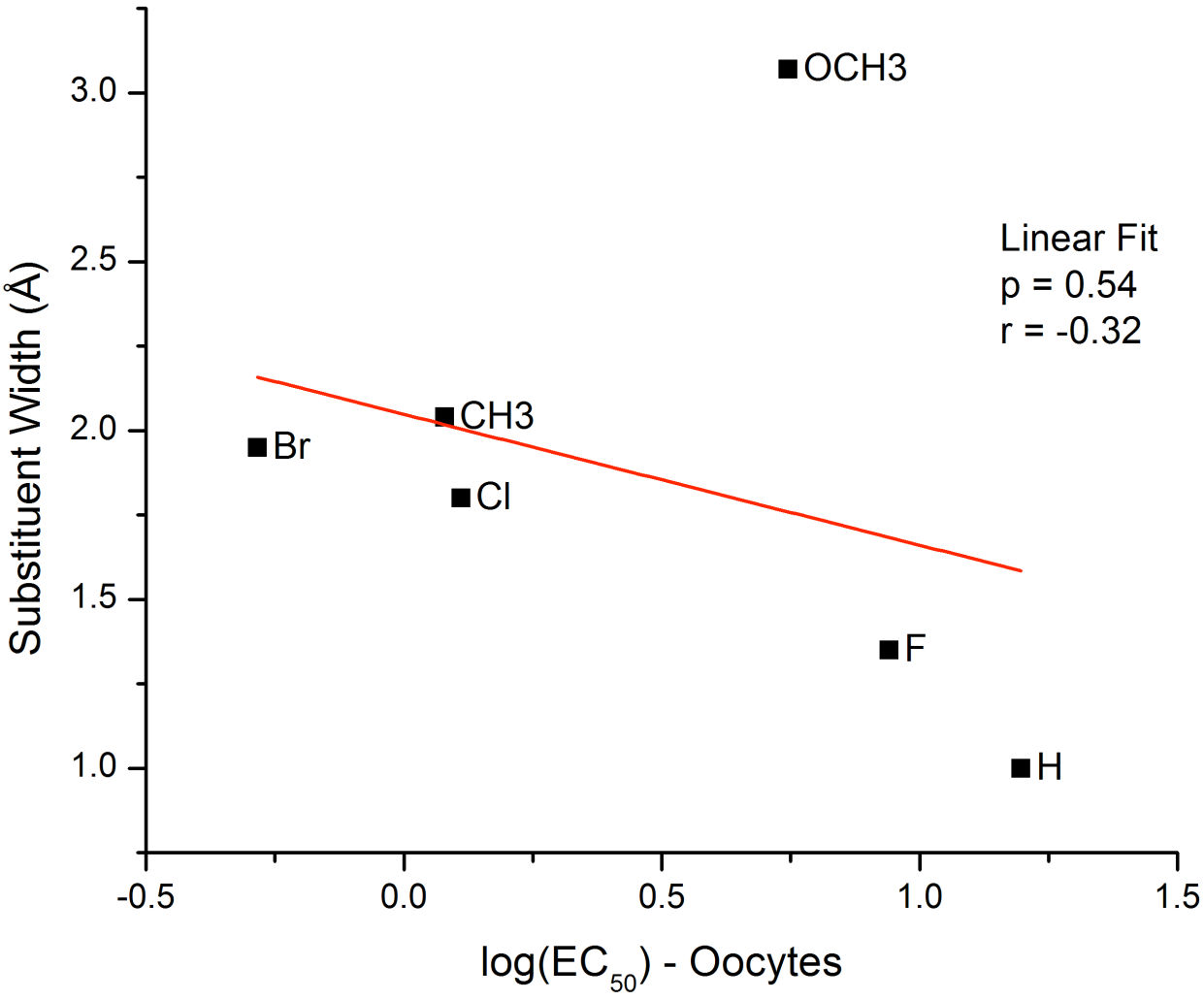

Figure 4.26: The EC_{50} values from concentration curves in oocytes correlated with each substituent's width, in angstroms. The results are statistically insignificant, r = -0.32 and p = 0.54. All values can be found in Table 4.14.

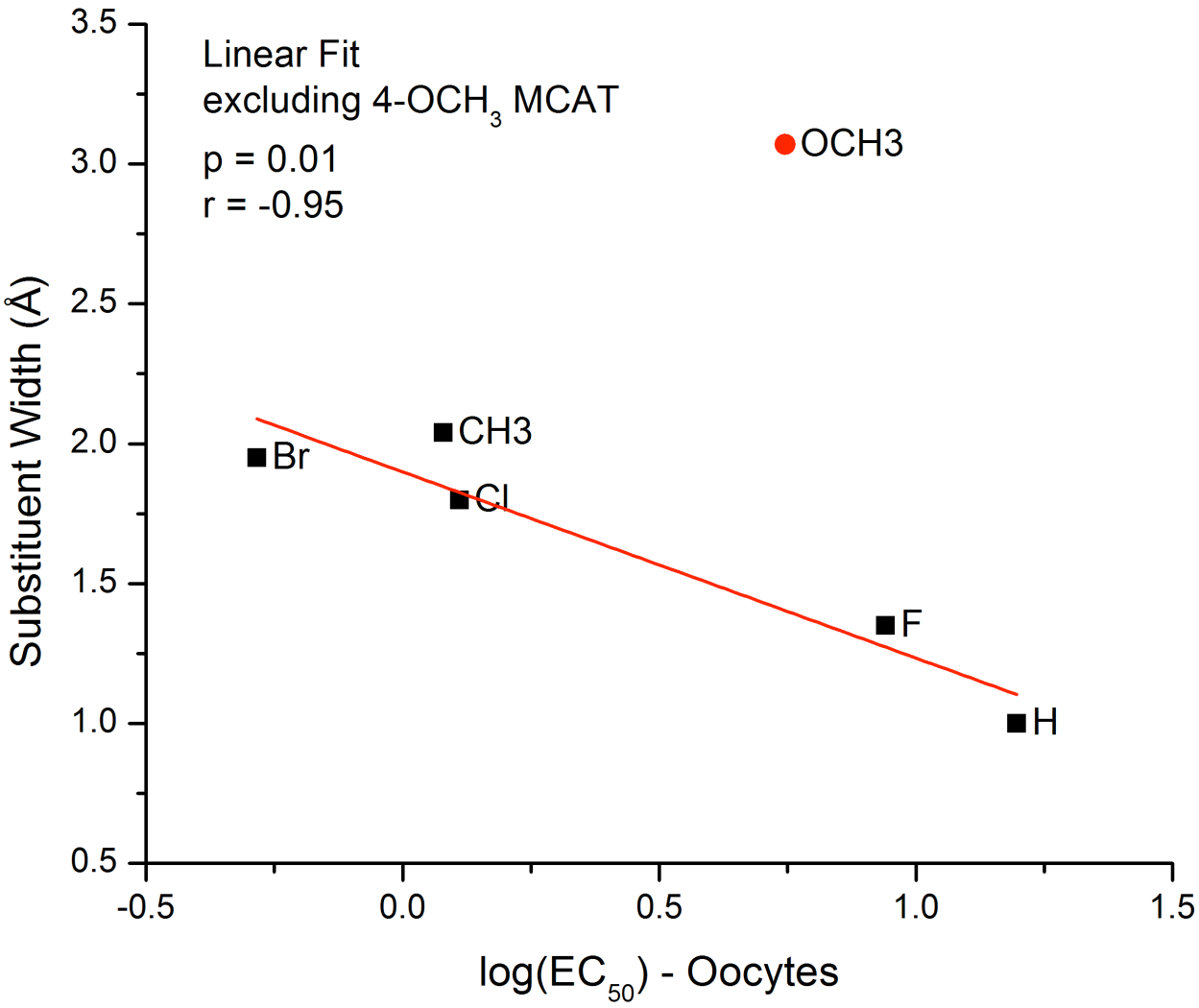

Figure 4.27: Correlational statistics between the EC_{50} values from concentration curves in oocytes and the width of each substituent, excluding methedrone (shown in red). The results of this correlation are statistically significant after excluding the methedrone outlier point ($r = -0.95$, $p = 0.01$).

Summary of Correlations Performed				
Variable A	Variable B	Significant?	R Value	P value
EC50 Values in Oocytes	EC50 Values in Synaptosomes	Yes	0.83	0.039
EC50 Values in Oocytes	Volume (Å^3)	No	-0.56	0.0026
EC50 Values in Oocytes (without methedrone)	Volume (Å^3)	Yes	0.992	0.0005
EC50 Values in Oocytes	Taft's E - Functional Steric Bulk	Yes	0.95	0.003
EC50 Values in Oocytes	Electron-Withdrawing Capacity	No	-0.445	0.377
EC50 Values in Oocytes	Lipophilicity	Yes	-0.933	0.004
Taft's E - Functional Steric Bulk	Volume (Å^3)	No	-0.65	0.16
Taft's E - Functional Steric Bulk (without methedrone)	Volume (Å^3)	Yes	-0.97	0.005
EC50 Values in Synaptosomes	Taft's E - Functional Steric Bulk	Yes	0.88	0.02
EC50 Values in Synaptosomes	Volume (Å^3)	Yes	-0.92	0.008
EC50 Values in Oocytes	Substituent Length (Å)	No	-0.61	0.19
EC50 Values in Oocytes (without methedrone)	Substituent Length (Å)	Yes	-0.96	0.01
EC50 Values in Oocytes	Substituent Maximum Width (Å)	No	-0.32	0.54
EC50 Values in Oocytes (without methedrone)	Substituent Maximum Width (Å)	Yes	-0.95	0.01

Table 4.28 : A summary of all correlational analyses performed. Results are listed here including the exact R and P values. Visual representations of each correlation can be found in Figures 4.15 – 4.27.

Discussion

Two different variations of the Hill equation were used to calculate maximum currents and EC_{50} values for the six 4-*para* substituted methcathinone compounds. The 'Hill' equation was fitted to flephedrone (4-F MCAT), brephedrone (4-Br MCAT), and clephedrone while the 'Hill1' equation was used for methcathinone (MCAT), methedrone (4-OCH_3 MCAT), and mephedrone (4-CH_3 MCAT). The Hill1 equation includes an offset and was used when the lowest concentration of each compound (0.1 micromolar) recorded was significantly greater than zero. Flephedrone, brephedrone, and clephedrone either elicited no response at the 0.1 micromolar concentration, or were trending toward zero and the Hill1 offset was not needed. Methcathinone required more data points for a proper Hill equation fit due to its high EC_{50} value. Recordings were taken at 0.1, 0.5, 1.0. 5.0, 10.0, 30.0, 50.0, and 100.0μM-drug concentrations for methcathinone.

Five of the six compounds were found to have reasonably similar maximum currents (between 84-113 nano-amps), while methedrone (4-OCH_3 MCAT) had a maximum current of 203.39 nano-amps. The much larger maximum current suggests that methedrone is much more efficacious at hSERT than the other compounds. In other words, methedrone is much better at opening the transporter and allowing current to flow thru regardless of potency at the transporter. The vast difference in maximal current adjusts methedrone's EC_{50} to the right on the graph – or makes it larger than expected. Baumann *et al*. (2012) and Bonano *et al.* (2014) simply looked at total release of serotonin in

synaptosomes caused by each compound. Methcathinone might have caused total release much quicker than the other compounds, but their experimental set up did not take into account the differences in time of release and efficacy of the compounds. This could possibly explain methcathinone's lack of correlation between oocyte and synaptosome data (seen in Figure 4.15). Methcathinone's degree of efficacy at the serotonin transporter could also have other effects, if repeatable in vivo. Is it possible that methcathinone might activate other transporters or channels as well due to its high degree of efficacy. For instance, the amount of current caused my methedrone acting on the serotonin transporter could be enough to activate surrounding calcium channels. Methedrone's effects at other related transporters would be an interesting continuation of this project, due to its high efficacy and possible potential for toxicity.

Each of the six compounds considered in this thesis produced concentration-dependent effects at hSERT. Brephedrone was shown to be the most potent compound eliciting effects on the serotonin transporter followed by (in order of potency) mephedrone, clephedrone, flephedrone, methedrone, and methcathinone. The Bonano *et al*. (2015) paper suggested that the larger the Taft's Steric E (E_S value), the more potent a compound would be for DAT instead of SERT. In other words, the E_S value is inversely related to the amount of steric bulk, and the lower the E_S value, the more potent the compound should be at hSERT. The SERT EC_{50} values in oocytes calculated from the data acquired for this thesis (Table 4.10) somewhat agree with the Bonano *et al*. paper. Methcathinone has the smallest functional steric bulk of the six compounds (E_S = 1.24), should be the most selective at DAT, and clearly is the least potent at SERT with a EC_{50} of 15.73. Methedrone (4-OCH_3 MCAT) appears to be the next least potent at SERT in our data

(EC_{50} = 5.56) and this almost agrees with the E_S value (0.69) where methedrone is the third highest. Bonano *et al*. found methedrone to be an outlier, having the most selectivity at SERT. The data here does not agree with Bonano *et al*.'s calculations of methedrone, and comes closer to following the predictions made from E_S values. Based on these E_S value predictions, flephedrone (4-F MCAT, E_S = 0.78) should be the second least potent at SERT behind methcathinone, but our data suggest that flephedrone (EC_{50} = 4.67,) is third least potent. Clephedrone (4-Cl MCAT, E_S = 0.27) has the next lowest E_S value, Bonano *et al*. calculated it to be the next highest in SERT selectivity, and our data (EC_{50} value of 1.29 [+/- 0.33]) agree. Mephedrone (4-CH_3 MCAT, E_S = 0) was found to be the second most potent compound at SERT in both data sets (EC_{50} = 1.20). Bonano *et al*. found brephedrone (4-Br MCAT) to be the most potent compound at SERT, while having the second lowest E_S value (0.08). Our data from oocyte concentration curves agrees with the Bonano *et al*. paper in that brephedrone (EC_{50} = 0.52) is the most potent compound at the hSERT transporter. In summary, the data collected for this thesis mostly agrees with Bonano *et al*. prediction that as the substituent's E_S value gets smaller the compound becomes more SERT selective.

Correlational statistical experiments were employed using the new EC_{50} values from the concentration-effect curves in oocytes. First, the new EC_{50} values from oocytes were calculated with the EC_{50} values from synaptosomes in Bonano *et al*. (2014) and Baumann *et al*. (2012) (all values can be found in Table 4.14). This resulted in a significant correlation between the two sets of EC_{50} values ($p = 0.039$, $r = 0.83$) suggesting that the concentration effect curve for each compound is similar in both xenopus oocytes and synaptosomes, and can be seen in Figure 4.15.

Next, a correlational analysis was performed between EC_{50} values from oocytes and a measure of volume for each 4-*para* substituted compound. These values of volume in cubic angstroms were borrowed from Sakloth, *et al*. 2015 and can also be found in Table 4.14. The correlation between volume and oocyte EC_{50} values is very weak but statistically significant with a p value of 0.0026 and an r value of -0.56, shown in Figure 4.16. When volume and EC_{50} values are plotted, like in Figure 4.16, it is obvious that one point is an outlier compared to the others. That data point is methedrone (4-OCH_3 MCAT), with the second highest EC_{50} value of 5.56 micromoles and the second lowest volume of 153.78 cubic angstroms. Another correlation was performed without methedrone's data point and the results differed drastically. Without methedrone, p = 0.0005 and r = 0.992, and can be seen in Figure 4.17. The stark contrast between the correlations of volume and EC_{50} values, with and without the methedrone data point, suggest that it could be an outlier. A correlation between volume and Taft's E (Figure 4.21) supports this theory because methedrone appears to be an outlier here as well. In order to explore why methedrone might be acting in such a way, the EC_{50} values were next correlated with the three parameters from Bonano *et al*. (2014): Taft's steric parameter, electron-withdrawing capacity, and lipophilicity.

Bonano *et al*. previously hypothesized that MCAT analogues with *para* substituents would demonstrate selectivity for either DAT or SERT, depending on the substituent (Bonano *et al*., 2015). In Bonano *et al*.'s paper, the only statistically significant correlation was found between selectivity at the transporters (or EC_{50} value) and functional steric bulk. To quantify steric bulk, Bonano *et al*. used Taft's steric parameter (E_S) which is calculated based on both steric strain and steric hindrance of each compound, as well as inductive,

resonance, and field influences (Bonano *et al.*, 2015). E_S values are indirectly related to the amount of functional steric bulk. In other words, the higher the E_S value, the lower the functional steric bulk of the substituent. The calculated E_S values can be found in Table 4.14. A correlation between the E_S values and the EC_{50} values produced an r value of 0.96 and a p value of 0.003, and can be seen in Figure 4.18. This is a strong correlational r value, and a p value less than 0.05, indicating a statistically significant correlation. It is interesting that the EC_{50} values in oocytes correlate well with the experimental Taft's E value but not volume, while the EC_{50} values from synaptosomes correlate with both.

The cause for methedrone (4-OCH_3 MCAT) being an outlier in the EC_{50} versus volume plot could potentially be caused by electronic factors of the substituent group. To explore this possibility, a correlation was performed between EC_{50} values and the electron-withdrawing capacity of each 4-*para* substituent compound. Methedrone possesses the lowest electron-withdrawing capacity (EWC = -0.27) and all the electron-withdrawing values can be found in Table 4.14. The correlation experiment returned a weak r value of -0.445 and a high p value of 0.377. These results, shown in Figure 4.19, suggest that electron-withdrawing capacity is not the cause of methedrone's aberrant placement on the EC_{50} vs. volume plot and methedrone's strangely weak potency at the serotonin transporter.

The relationship between the EC_{50} value of each compound and lipophilicity was correlated and the resulting values, r = -0.933 and p = 0.004, propose a significant statistical relationship between the lipophilcity and the EC_{50} value of each compound. Figure 4.20 illustrates the correlation and suggests that the liophilicity of each 4-*para* substituted methcathinone compound could influence the respective EC_{50} values.

The EC_{50} values obtained by Baumann *et al.* (2012) in synaptosomes correlate strongly with both Taft's E (Figure 4.22, r = 0.88, p = 0.02) and volume (Figure 4.23, r = -0.92, p = 0.008). The EC_{50} values from oocytes correlate with EC_{50} values from synaptosomes, but not with volume and Taft's E signifying a difference modulating EC_{50} values in oocytes that does not exist in synaptosomes. Oocyte EC_{50} values have been shown to correlate well with values of substituent length and width, (Figures 4.25, 4.27) similar to synaptosomes when excluding methedrone. Thus the discrepancies in EC_{50} values between synaptosomes and oocytes could be caused by a difference in expression, protein packaging, or modification and previous experiments have shown differing EC_{50} values in *Xenopus* oocytes when compared to values in rat syaptosomes (Dowd *et al.* 1996).

In conclusion, each of the six 4-*para* substituted methcathinone compounds elicit a distinct response at the human serotonin transporter. The particular substitution made at the 4-position on the benzyl ring influences the overall potency at the serotonin transporter, and the size of the substitution clearly is a factor. Substituent volume does not correlate perfectly though, as shown by the outlier methedrone (4-OCH_3 MCAT). The experimental measurement of Taft's E, which takes into account volume, is more predictive of methcathinone analog efficicay at hSERT and the data suggest other factors are also at play. Electron-withdrawing capacity was shown to have no direct influence on efficacy and EC_{50} values. However, the lipophilicity of each compound provided a significant correlation to the EC_{50} values found from oocyte concentration-curves. These results imply the general rule: the larger the overall volume of the compound, the more efficient that compound will be at the serotonin transporter (compared to the dopamine transporter), when expressed in oocytes. Outliers are possible due to other factors including lipophilicity (and excluding

steric bulk and electron-withdrawing capacity) and the results differ in other assays such as rat synaptosome experiments. Such dissimilarities could be due to varying membrane lipid and protein compositions in the different cell types or any number of pre or post-translational modifications to the transporter. We can conclude that measurements of volume, substituent size, and steric bulk are indirectly related to methcathinone analogue potency at the human serotonin transporter, possibly modulated in part by the compound's lipophilicity and other unknown factors.

Literature Cited

Baumann, M., Ayestas, M., Partilla, J., Sink, J., Shulgin, A., Daley, P., Brandt, S., Rothman, R., Ruoho, A., Cozzi, N. (2012). The designer methcathinone analogs, mephedrone and methylone, are substrates for monoamine transporters in brain tissue. Neuropsychopharmacology, 37: 1192–1203.

Baumann, M., Solis, E., Watterson, L., Marusich, J., Fantegrossi, W., Wiley, J. (2014). Bath Salts, Spice, and Related Designer Drugs: The Science Behind the Headlines. The Journal of Neuroscience, November 12, 2014.

Bengel, D., Murphy, D., Andrews, A., Wichems, C., Feltner, D., Heils, A., Mossner, R., Westphal, H., and Lesch, K. [1998]. Altered brain serotonin homeostasis and locomotor insensitivity to 3,4-methylenedioxymethamphetamine ("Ecstasy") in serotonin transporter-deficient mice. Mol Pharmacol 53:649 – 655.

Berger, M., Gray, J., Roth, B. (2009). The Expanded Biology of Serotonin. Annual Reviews of Medicine, 2009.60:355-366.

Beuming, T., Shi, L., Javitch, J., Weinstein, H. (2006). A Comprehensive Structure-Based Alignment of Prokaryotic and Eukaryotic Neurotransmitter/Na^+ Symporters (NSS) Aids in the Use of the LeuT Structure to Probe NSS Structure and Function.

Bierwirtz, A., Schwarz, W. (2014). Two-electrode voltage-clamp (TEVC). Biophysikalisches Praktikum, Institute für Biophysik, Johann Wolfgang Goethe-Universität, 2014. http://www.biophys.unifrankfurt.de/~wille/prakt/anleitungen/03_elektrophys.pdf

The Biology Project (2007). Rational Function Applications, Hill Equation. Department of Biochemistry and Molecular Biophysics, University of Arizona. http://www.biology.arizona.edu

Billesbølle, C., Krüger, M., Shi, L., Quick, M., Li, Z., Stolzenberg, S., Kniazeff, J., Gotfryd, K., Mortensen, J., Javitch, J., Weinstein, H., Loland, C., Gether, U. [2015]. Substrate-induced Unlocking of the Inner Gate Determines the Catalytic Efficieny of a Neurotransmitter: Sodium Symporter. The Journal of Biological Chemistry. Vol:290, No.44.

Blakely, R., Ramamoorthy, S., Schroeter, S., Qian, Y., Apparsundaram, S., Galli, A., De Felice, J. (1998). Regulated phosphorylation and trafficking of antidepressant-sensitive serotonin transporter proteins, Biological Psychiatry, Volume 44, Issue 3, 1 August 1998, Pages 169-178, ISSN 0006-3223, http://dx.doi.org/10.1016/S0006-3223(98)00124-3.

Bonano, J., Banks, M., Kolanos, R., Sakloth, F., Barnier, M., Glennon, R., Cozzi, N., Partilla, J., Baumann, M., Negus, S. (2015). Quantitative structure-activity relationship analysis of the pharmacology of *para*-substituted methcathinone analogues. 2015. British Journal of Pharmacology, 172, p.2433.

Bruns, D., Engert, F., Lux, H. (1993). A fast activating presynaptic reuptake current during serotonergic transmission in identified neurons of Hirudo. Neuron 10:559—72.

Cameron, K., Kolanos, R., Solis, E., Glennon, R., De Felice, L. (2013). Bath salts components mephedrone and methylenedioxypyrovalerone (MDPV) act synergistically at the human dopamine transporter. *British Journal of Pharmacology*. 2013;168(7):1750-1757. doi:10.1111/bph.12061.

Cameron, K., Solis, E. Jr., Ruchala, I., De Felice, L., Eltit, J. (2015). Amphetamine activates calcium channels through dopamine transporter-mediated depolarization, Cell Calcium, Volume 58, Issue 5, November 2015, Pages 457-466, ISSN 0143-4160, http://dx.doi.org/10.1016/j.ceca.2015.06.013.

Carroll, F. [2003]. Medicinal Chemistry Division Award address 2002: monoamine transporters and opioid receptors. Targets for addiction therapy. J Med Chem 46:1775–1794.

Cheng, M. and Bahar, I. (2015). Molecular Mechanism of Dopamine Transport by Human Dopamine Transporter. http://dx.doi.org/10.1016/j.str.2015.09.001.

Coleman, J., Green, E., Gouaux, E. (2016). X-ray structures and mechanism of the human serotonin transporter. Nature, vol. 532, 334-339. doi:10.1038/nature17529

Dascal, N., Landau, E., Lass, Y. (1984). Xenopus oocyte resting potential, muscarinic responses and the role of calcium and guanosine 3',5'-cyclic monophosphate.. The Journal of Physiology, 352 doi: 10.1113/jphysiol.1984.sp015310.

De Felice L., Adams, S., Ypey, D. (2001). Single-file diffusion and neurotransmitter transporters: Hodgkin and Keynes model revisited. BioSystems 62:57– 66.

De Felice, L. (2004). Going Against the Flow. Nature 2004, 432, 279.

De Felice, L., Goswami, T. (2007). *Transporters as Channels*. Annual Review of Physiology, 2007. 69:87-112.

De Felice, L., Glennon, R., Negus, S. (2014). Synthetic cathinones: chemical phylogeny, physiology, and neuropharmacology. Life Science, 2014. 97:20 –26.

De Felice, L. (2016). Chloride requirement for monoamine transporters. Pflugers Arch – European Journal of Physiology. dio: 10.1007/s00424-015-1783-4

Dowd, L., Coyle, A., Rothstein, J., Pritchett, D., Robinson, M. (1996). Comparison of Na+-dependent glutamate transport activity in synaptosomes, C6 glioma, and Xenopus oocytes expressing excitatory amino acid carrier 1 (EAAC1). MolPharmacol 49: 465–473.

Eshleman, A., Wolfrum, K., Hatfield, M., Johnson, R., Murphy, K., Janowsky, A. (2013). Substituted methcathinones differ in transporter and receptor interactions. Biochem Pharmacol 85:1803–1815.

Findlay, J., Warren, J., Hill, J., Welch, R. (1981). Stereospecific radioimmunoassays for d-pseudoephedrine in human plasma and their application to bioequivalency studies. J Pharm Sci 70: 624-631.

Foley, K., Cozzi, N. (2003). Novel aminopropiophenones as potential antidepressants. Drug Dev Res 60: 252-260.

Forest, L., and Rudnick, G. [2009]. The rocking bundle: a mechanism for ion-coupled solute flux by symmetrical transporters. *Physiology (Bethesda)* 24:377-386.

Guan, B., Chen, X., Zhang, H. (2013). Two-electrode voltage clamp. Methods Mol Biol , 2013, Vol.998, p.79-89

Guastella, J., Nelson, N., Nelson, H., Czyzyk, L., Keynan, S., Miedel, M., Davidson, N., Lester, H., and Kanner, B. [1990]. Cloning and expression of a rat brain GABA transporter. Science 249:1303–1306.

Hahn, M. and Blakely, R. (2007). The Functional Impact of SLC6 Transporter Genetic Variation. The Annual Review of Pharmacology and Toxicology. 2007.47:401-441.

Hediger, M., Romero, M., Peng, J., Rolfs, A., Takanaga, H., and Bruford, E. [2004]. The ABCs of solute carriers: physiological, pathological, and therapeutic implications of human membrane transport proteins. Pflugers Arch 447:465– 468.

Hirsch, M. and Birnbaum, R. [1] Tricyclic and Tetracyclic Drugs: Pharmacology, administration, and side effects. UpToDate Database. http://www.uptodate.com/contents/tricyclic-and-tetracyclic-drugs-pharmacology-administration-and-sideeffects

Hirsch, M. and Birnbaum, R. [2] Selective Serotonin Reptake Inhibitors: Pharmacology, administration, and side effects. UpToDate Database.

http://www.uptodate.com/contents/selective-serotonin-reuptake-inhibitors-pharmacology-administration-and-side-effects

Humphreys, C., Wall, S., and Rudnick, G. [1994]. Ligand Binding to the Serotonin Transporter: Equilibria, Kinetics, and Ion Dependence. *Biochemistry* 1994 *33* (31), 9118-9125.

Jardetzky, O. [1966]. Simple allosteric model for membrane pumps. *Nature* 211:969-970.

Jin, C., Navarro, H., and Carroll, F. [2008]. Development of 3-phenyltropane analogues with high affinity for the dopamine and serotonin transporters and low affinity for the norepinephrine transporter. J Med Chem 51:8048 – 8056.

Kilic, F., Murphy, D., and Rudnick, G. [2003]. A human serotonin transporter mutation causes constitutive activation of transport activity. Mol Pharmacol 64:440 – 446.

Kristensen, A., Andersen, J., Jorgensen, T., Sorensen, L., Eriksen, J., Loland, C., Strømgaard, K., and Gether, U. (2011). SLC6 neurotransmitter transporters: structure, function, and regulation. Pharmacol. Rev. 63, 585–640. 10.1124/pr.108.000869

Lespagnol, A., Hallot, J. (1954). Preparation of p-methozyephedrone. Bulletin de la Societe de Pharmacie de Lille 45-46.

Machaca, K., Hartzell, H.. (1998). Asymmetrical distribution of Ca-activated Cl channels in Xenopus oocytes. *Biophysical Journal*. 1998;74(3):1286-1295.

Mager, S., Min, C., Henry, D., Chavkin, C., Hoffman, B., Davidson, N., Lester, H. (1994). Conducting States of a Mammalian Serotonin Transporter. Division of Biology, California Institute of Technology. Cell Press, 1994, Neuron, Vol. 12, 845-859.

Maisto, S., Galizio, M., Connors, G. (2007). Drug Use and Abuse. 6th ed. Belmont: Wadsworth. Print.

Malinauskaite, L., Quick, M., Reinhard, L., Lyons, J., Yano, H., Javitch, J., Nissen, P. [2014]. A mechanism for intracellular release of Na+ by neurotransmitter/sodium symporters. Nature Structural and Molecular Biology. Vol:21, 11.

McDermott, S., Power, J., Kavanagh, P., O'Brien, J. (2011). The analysis of substituted cathinones. Part 2: an investigation into the phenylacetone based isomers of 4-methylmethcathinone and N-ethylcathinone. Forensic Sci Int 212: 13-21.

Manepalli, S., Surratt, C., Madura, J., Nolan, T. (2012). Monoamine Transporter Structure, Function, Dynamics, and Drug Discovery: A Computational Perspective. Department of Chemistry and Biochemistry, Center for Computational Sciences, Duquesne University, Pittsburgh, Pennsylvania, USA.

Miller, A., Zhou, J. (2000). Xenopus oocytes as an expression system for plant transporters, Biochimica et Biophysica Acta (BBA) - Biomembranes, Volume 1465, Issues 1–2, 1 May 2000, Pages 343-358, ISSN 0005-2736, http://dx.doi.org/10.1016/S0005-2736(00)00148-6.

Mitchell, P. [1990]. Osmochemistry of solute translocation. *Res Microbiol* 141:286-289.

Prasad, H., Zhu, C., McCauley, J., Samuvel, D., Ramamoorthy, S., Shelton, R., Hewlett, W., Sutcliffe, J., and Blakely R. [2005] Human serotonin transporter variants display altered sensitivity to protein kinase G and p38 mitogen-activated protein kinase. Proc Natl Acad Sci USA 102:11545–11550.

Rothman, R., Baumann, M. (2003). Monoamine transporters and psychostimulant drugs. Eur J Pharmacol 479:23–40.

Rothman, R., Baumann, M. (2006). Balance between dopamine and serotonin release modulates behavioral effects of amphetamine-type drugs. Ann N Y Acad Sci 1074:245–260.

Sakloth, F., Kolanos, R., Mosier, P., Bonano, J., Banks, M., Partilla, J., Baumann, M., Negus, S., Glennon, R. (2014). Steric parameters, molecular modeling and hydropathic interaction analysis of the pharmacology of para-substituted methcathinone analogues. British Journal of Pharmacology. 172, 9, 1476-5381. DOI: 10.1111/bph.13043

Schechter, M., Glennon, R. (1985). Cathinone, cocaine and methamphetamine: similarity of behavioral effects. Pharmacol Biochem Behav 22: 913–916.

Sigel, E. (2010). Microinjection into Xenopus Oocytes. In: eLS. John Wiley & Sons Ltd, Chichester. http://www.els.net [doi: 10.1002/9780470015902.a0002658.pub2]

Singh, S., Yamashita, A., Gouaux, E. [2007]. Antidepressant binding site in a bacterial homologue of neurotransmitter transporters. Nature Publishing Group, 2007. Vol: 448.

The Smithsonian, National Zoological Park - Reptiles & Amphibians, African Clawed Frog. http://nationalzoo.si.edu/Animals/ReptilesAmphibians/Facts/FactSheets/Africanclawedfrog.cfm

Stolzenberg, S., Quick, M., Zhao, C., Gotfryd, K., Khelashvili, G., Gether, U., Loland, C., Javitch, J., Noskov, S., Harel, W., Shi, L. [2015]. Mechanism of the Association between Na+ Binding Conformations at the Intracellular Gate in Neurotransmitter: Sodium Symporters. The Journal of Biological Chemistry. Vol:290, No 22, pp. 13992-14003.

Trepanier, D., Sprancmanis, V. (1964). 5,6-Dihydro-4H-1,3,4-oxadiazines. II. Structural requirements for effective hydrazido-hydroxyl interaction. J Org Chem 29: 673-677.

U.S. Drug Enforcement Administration, United States Department of Justice. Drug Scheduling. http://www.dea.gov/druginfo/ds.shtml

Wolff, M. (1980). The quantitative analysis of structure-activity relationships. In: Wolff ME (ed.). Burger's Medicinal Chemistry, 4th edition. Wiley: New York, pp. 393-418.

Yamashita, A., Singh, S., Toshimitsu, K., Jin, Y., and Gouaux, E. [2005]. Crystal structure of a bacterial homologue of Na^+/Cl^--dependent neurotransmitter transporters. *Nature* 437, 215-223 (8 September 2005).

Zawilska, J., Wojcieszak, J. (2013). Designer cathinones: an emerging class of novel recreational drugs. Forensic Sci Int 231:42–53.